Generalized two-layer models of ocean circulation

by Rick Salmon[1]

ABSTRACT

The assumption that surfaces of constant temperature and potential vorticity coincide leads to an exact, time-dependent reduction of the ideal thermocline equations in an ocean basin of arbitrary shape. After modifications to include forcing, dissipation, and the presence of the equator, these reduced equations form the basis for numerical models that are both more realistic and easier to solve than the conventional two-layer model.

1. Introduction

Like many equations in fluid mechanics, the ideal thermocline equations, (2.1–2) in standard notation, comprise a system of quasi-linear, first-order partial differential equations. Such systems are amenable to the method of characteristics, but only in the case of two independent variables.[2] Unfortunately, the ideal thermocline equations contain the four independent variables (x, y, z, t). However, time-independent solutions of (2.1–2) are frequently of interest; this reduces the number of independent variables to three.

In layered models of the ocean circulation, one assumes that the ocean consists of immiscible layers of uniform density, separated by meniscuses at which the density is discontinuous. A second independent variable (z) is thereby removed at the relatively low cost of increasing the number of dependent variables, which then include the layer thicknesses. In steady state, the layered models depend only on (x, y), and the method of characteristics therefore applies in regions of negligible dissipation (where the equations are, approximately, first-order). These facts underlie the many relatively successful analytical attacks on layered equations (see, for example, Luyten *et al.* (1983) for an important and influential example). The theory of (2.1–2) is comparatively meager.

In this paper, we show that layered models are neither the only, nor probably the best, method for reducing the number of independent variables in (2.1–2). In particular, we consider solutions of the form

$$\theta = \Theta\left(\frac{z}{y} + S(x, y, t)\right) \tag{1.1}$$

1. Scripps Institution of Oceanography, La Jolla, California, 92093-0225, U.S.A.
2. For a discussion of this point, see for example Whitham (1974, p. 139).

where θ is the temperature, $\Theta(\ )$ is an *arbitrarily* prescribed function of a single variable, and $S(x, y, t)$ remains to be determined. The other symbols have their usual meanings, explained fully below. We call $\Theta(\ )$ the *profile function* of the model. The physical interpretation of S depends on the choice of profile function, but if, as in nearly all of the cases we consider, $\Theta(\xi)$ or its derivative is discontinuous at $\xi = 0$, then $z = -yS$ is the vertical location of this discontinuity, and (taking $z = 0$ to be the ocean surface) $h \equiv yS$ is the thickness of the fluid layer above it.

Our fundamental ansatz (1.1) is equivalent to the assumption that surfaces of constant θ and potential vorticity $y\theta_z$ coincide. Such special assumptions have been common in oceanography, beginning perhaps with Welander's (1971) seminal paper. Indeed, Needler (1971) investigated solutions of the general form (1.1), anticipating some of the results in Sections 2 and 3 below. Cushman-Roisin (1984) and others have investigated solutions of the form (1.1) with $\Theta(\ )$ chosen to be an exponential function. In this paper, we show how (1.1) forms the basis for a simple, full-basin circulation model in an ocean with arbitrary bottom topography, and we present numerical solutions for several realistic choices of $\Theta(\ )$.

In Section 2, we confirm that (1.1) is consistent with the ideal thermocline equations (2.1–2) *and* with boundary conditions of no-normal-flow at the ocean surface and bottom, in the sense that substitution of (1.1) into (2.1–2) and its boundary conditions (2.9–10) yields an evolution equation, (2.19), for $S(x, y, t)$, in which the vertical coordinate, z, does not appear. This evolution equation contains a second dependent variable, the transport streamfunction $\psi(x, y, t)$, for which another z-independent equation, (2.17), must be developed. The ideal thermocline equations (2.1–2) and their boundary conditions are then satisfied by solutions of (2.17, 19). If the arbitrary function $\Theta(\ )$ in (1.1) is a step-function, then (2.17, 19) reduce to the conventional (ideal) equations (2.28, 29) for a two-layer fluid, where $h = yS$ is the depth of the upper layer. We therefore call (2.17, 19) the (ideal form of the) *generalized two-layer equations* (GTLE).

Although the conventional two-layer equations form the basis for many analytical studies of large-scale circulation, they have two important disadvantages: First, numerical solution is difficult when the meniscus between layers intersects the ocean surface or bottom; and, second, the observed ocean does not closely resemble a system of two homogeneous layers.

The GTLE based on (1.1) offer a way to overcome both difficulties. If two homogeneous layers are really wanted, then the step-function can be replaced by a $\Theta(\ )$ that varies rapidly but *continuously* between the temperature values of the layers. The surface intersection of the boundary between layers is then a region of rapid but continuous temperature change, whose precise location need not be explicitly followed. This overcomes the technical numerical difficulty of following the outcropping meniscus in the conventional two-layer model. However, the observed ocean more closely resembles two layers with different, nonzero stratifications

separated by a smooth transition, than it does two layers of uniform density separated by a sharp jump. In this paper we show that a more realistic choice of $\Theta(\ )$ yields solutions that better resemble the ocean, without cancelling any of the other advantages of the conventional two-layer formulation. Those other advantages are maintained because the reduction to two independent variables—by whatever means—allows the method of characteristics to apply.

In Section 3, we illustrate the power of the method of characteristics by constructing the general steady solution of the ideal GTLE. This solution generalizes the result of an earlier paper (Salmon, 1992; hereafter S92) for the conventional case of two homogeneous layers. For the conventional two-layer case, S92 proposed a particular steady solution that resembles the flow along the continental slope east of North America. In this solution, a frictional internal boundary layer containing a strong southward flow separates a seaward region of uniform upper-layer potential vorticity from a landward, Gulf Stream region of uniform lower-layer potential vorticity. Now, all of the results of S92 extend to the GTLE, which are however much more amenable to numerical solution than are the conventional two-layer equations. Thus, the GTLE may help to settle the question of whether solutions like those proposed by S92 actually occur as pieces of whole-basin solutions with realistic forcing and dissipation. This motivated the present study.

Unfortunately, forcing and dissipation destroy the special status of the ansatz (1.1). That is, (1.1) is not precisely consistent with the generalization (4.1–2) of (2.1–2) to include forcing and dissipation. As explained in Section 4, the only recourse is to admit the forcing and dissipation as a Galerkin-type projection onto the ideal dynamics. (A similar procedure removes the singularity in (1.1) at the equator, $y = 0$.) The resulting equations, (4.4, 31), generalize the GTLE to include forcing and dissipation terms. This strategy of projecting *nonconservative* effects onto a flow representation, (1.1), chosen for its special relationship to the *conservative* dynamics is really the same strategy followed in the conventional two-layer formulations, where (for example) one replaces the wind-forcing by a vertically uniform body-force in the upper layer, to preserve the assumed depth-independence of horizontal flow in each layer, and where (to give another example) one sometimes models the vertical diffusion of temperature as an exchange of mass between layers, ignoring the fact that real diffusion would smooth out the sharp temperature jump between layers. Outside the equatorial region, and outside regions with significant dissipation, solutions based on (1.1) retain their two special properties: they are exact solutions of the corresponding three-dimensional equations (2.1–2), and they are amenable to the method of characteristics. Inside the equatorial region, and inside boundary- and internal-layers with significant dissipation, our final equations have the status of an ordinary Galerkin approximation.

Following a brief discussion, in Section 5, of some previous work on the conventional two-layer model in oceans with uniform depth, we turn in Section 6 to

numerical solutions of the GTLE in a model ocean bounded on three sides by
coastlines at which the ocean depth vanishes smoothly. The southern, equatorial
boundary is open, and cross-equatorial symmetry is assumed. The numerical calcula-
tions show that the torque resulting from the joint effect of baroclinicity and
topography greatly increases the depth-averaged component (i.e., the ψ-component)
of the circulation, and causes a northward extension of the Gulf Stream along the
western continental slope. The baroclinic, S-component of the circulation is very
sensitive to the imposed forcing and, particularly, to the prescribed volume of warm
"upper layer" fluid. This sensitivity can be partly understood by mapping the
characteristic velocity of the general S-equation (4.31). This characteristic velocity—
the velocity at which information about temperature or potential vorticity flows from
one region to another—has three principal components. One component is the
depth-averaged velocity; a second component corresponds to westward propagation
at the speed of internal Rossby waves; the third component parallels the isobaths, in
the direction of topographic Rossby waves. When the total volume of warm water is
relatively large, the westward Rossby propagation predominates in mid-ocean, the
North Atlantic Current shifts toward the western boundary, and there is relatively
little cold water outcropping in the subpolar gyre. When the total volume of warm
water is relatively small, the eastward depth-averaged flow predominates in the
subpolar gyre, the North Atlantic Current shifts southward and eastward, and the
area of cold-water outcrop is large. Shock layers in the temperature field occur along
lines at which the characteristic velocity converges. The characteristic velocity is thus
a useful diagnostic tool, but it is no substitute for a completely deductive theory of
the GTLE. Concluding remarks in Section 7 emphasize the shortcomings of the
current numerical implementation and the prospects for such a theory.

2. Generalized two-layer dynamics

Our starting point is the ideal thermocline equations—or, as they are coming to be
called, the *planetary geostrophic equations*—which, in nondimensional form, and
temporarily omitting all forcing and dissipation terms, are

$$
\begin{aligned}
-fv &= -\phi_x \\
fu &= -\phi_y \\
0 &= -\phi_z + \theta \\
u_x + v_y + w_z &= 0
\end{aligned}
\tag{2.1}
$$

and

$$
\theta_t + u\theta_x + v\theta_y + w\theta_z = 0.
\tag{2.2}
$$

As usual (u, v, w) is the velocity in the (east, north, vertical) direction with coordinate
(x, y, z), ϕ is the pressure, θ the buoyancy (which we will call temperature), t the time,
$f = y$ is the Coriolis parameter, and coordinate subscripts denote differentiation.

The ideal equations (2.1–2) conserve the temperature θ and the potential vorticity $y\theta_z$ on fluid particles. Thus, if at some initial time

$$y\theta_z = G(\theta) \tag{2.3}$$

where G is an *arbitrary* function of a single argument, then (2.3) holds at all future times. This is true even in the presence of a rigid horizontal lid and a nonvertical bumpy bottom, because (as we see below) the boundary condition of no-normal-flow at such boundaries can be satisfied by the dynamics (2.1–2) without the need for dissipation (which would destroy the conservation of temperature and potential vorticity).

Solving (2.3) for θ, we find that

$$\theta = F''\left(\frac{z}{y} + S(x, y, t)\right) \tag{2.4}$$

where F'' ($\equiv \Theta$) is another arbitrary function, related to G, and the primes, which denote differentiation, are introduced for later convenience. Again, (2.4) is the basic ansatz of this paper. To obtain the equation governing $S(x, y, t)$, we substitute (2.4) back into (2.1–2). First recall that every solution of (2.1) can be written in the form

$$\phi = M_z, \qquad \theta = M_{zz}, \qquad u = -\frac{1}{y}M_{zy}, \qquad v = \frac{1}{y}M_{zx}, \qquad w = \frac{1}{y^2}M_x \tag{2.5}$$

where $M(x, y, z, t)$ is Welander's potential function. Substituting (2.5) into (2.2), we obtain the familiar equation,

$$M_{zzt} - \frac{1}{y}M_{zy}M_{zzx} + \frac{1}{y}M_{zx}M_{zzy} + \frac{1}{y^2}M_xM_{zzz} = 0. \tag{2.6}$$

Now, two integrations of (2.4) yield

$$M = y^2 F\left(\frac{z}{y} + S(x, y, t)\right) + zP(x, y, t) + D(x, y, t) \tag{2.7}$$

where $S(x, y, t), P(x, y, t)$ and $D(x, y, t)$ must all be determined. Substituting (2.7) into (2.6), we obtain the evolution equation for $S(x, y, t)$,

$$S_t + \frac{1}{y}J(P, S) + \frac{1}{y^3}D_x = 0 \tag{2.8}$$

where $J(A, B) \equiv A_xB_y - A_yB_x$ is the horizontal Jacobian. To obtain equations for $P(x, y, t)$ and $D(x, y, t)$, we apply the no-normal-flow boundary conditions at the ocean surface,

$$w = 0 \qquad \text{at} \qquad z = 0 \tag{2.9}$$

and bottom,

$$w = -uH_x - vH_y \quad \text{at} \quad z = -H(x, y).$$

(2.10)

By (2.5) and (2.7), (2.9) is

$$y^2 F'(S)S_x + D_x = 0$$

(2.11)

so that (2.8) becomes

$$\frac{\partial S}{\partial t} + \frac{1}{y}J(P, S) - \frac{1}{y}\frac{\partial}{\partial x}F(S) = 0.$$

(2.12)

The bottom boundary condition (2.10) will now be satisfied if

$$\nabla \cdot \left[\int_{-H}^{0} (u, v)\, dz \right] = 0$$

(2.13)

that is, if

$$\int_{-H}^{0} u\, dz = -\psi_y \quad \text{and} \quad \int_{-H}^{0} v\, dz = \psi_x$$

(2.14)

for some $\psi(x, y, t)$. By (2.5) and (2.7), (2.14) are

$$2F\left(S - \frac{H}{y}\right) - 2F(S) + \left[\frac{H}{y} + yS_y\right]F'\left(S - \frac{H}{y}\right) - yS_y F'(S) - \frac{H}{y}P_y = -\psi_y \quad (2.15)$$

and

$$yS_x\left[F'(S) - F'\left(S - \frac{H}{y}\right)\right] + \frac{H}{y}P_x = \psi_x.$$

(2.16)

Eliminating ψ between (2.15–16) yields a second equation for P and S. However, it is more convenient to use the transport streamfunction $\psi(x, y, t)$ instead of $P(x, y, t)$. Eliminating P between (2.15–16), we obtain the equation for ψ,

$$J\left(\psi, \frac{y}{H}\right) + J\left(\frac{1}{H}, \gamma\right) = 0$$

(2.17)

where

$$\gamma = y^2\left[F(S) - F\left(S - \frac{H}{y}\right) - \frac{H}{y}F'\left(S - \frac{H}{y}\right)\right] = -\int_{-H}^{0} z\theta\, dz.$$

(2.18)

The last equality in (2.18) follows from (2.4). Then, solving (2.15–16) for P_x and P_y, and substituting the result into (2.12), we obtain the S-equation in the form

$$H\frac{\partial S}{\partial t} + J(\psi, S) + c\frac{\partial S}{\partial x} = 0$$

(2.19)

where

$$c \equiv 2F(S) - 2F\left(S - \frac{H}{y}\right) - \frac{H}{y}F'(S) - \frac{H}{y}F'\left(S - \frac{H}{y}\right) \tag{2.20}$$

and c/H is the internal Rossby phase speed. Note, using (2.4), that

$$c = \frac{1}{y^2}\int_{-H}^{0} z(z + H)\theta_z\, dz < 0 \tag{2.21}$$

corresponding to westward phase propagation (for a statically stable profile function).

For given $F(\ )$, (2.17, 19) are closed equations for $\psi(x, y, t)$ and $S(x, y, t)$ whose solutions correspond to exact solutions of the ideal thermocline equations (2.1–2) in an ocean of depth $H(x, y)$, with boundary conditions of no-normal-flow. The evolution equation (2.19) for S is analogous to (2.2); S determines the three-dimensional temperature field by (2.4). Given $S(x, y, t)$, (2.17) determines ψ, and hence (u, v, w), in the same way that (2.1) and the surface- and bottom-boundary conditions determine the three-dimensional velocity field from θ. However, neither (2.1) nor (2.17) can satisfy the *coastal* boundary condition $\psi = 0$ at $H = 0$ unless friction is added to the horizontal momentum equations in (2.1). That is, although friction is not required to prevent flow through the ocean surface or bottom, it *is* required to prevent a mass flux through the cusp at $H = 0$. The friction converts the hyperbolic equation (2.17) into an elliptic equation for ψ. We defer further discussion of friction to Section 4, where we address the general problem of adding forcing and dissipation to the dynamics (2.17, 19). In the remainder of this section, we consider some special cases of the ideal-fluid dynamics (2.17, 19) corresponding to particular choices of the profile function F''.

Surely the simplest case of (2.4) is the case of *uniform temperature*, $F \equiv 0$, for which (2.17) reduces to $J(\psi, y/H) = 0$ and (2.19) dissolves.[3] More interesting is the case of *uniform potential vorticity*, $y\theta_z = Q$ (constant), corresponding to

$$F(\xi) = \tfrac{1}{6}Q\xi^3 \tag{2.22}$$

for which, defining $T(x, y, t) \equiv QS(x, y, t)$, (2.4) becomes

$$\theta = Q\frac{z}{y} + T(x, y, t) \tag{2.23}$$

and (2.17, 19) reduce to

$$J\left(\psi, \frac{y}{H}\right) - J\left(H, \frac{1}{2}T - \frac{1}{3}Q\frac{H}{y}\right) = 0 \tag{2.24}$$

---

3. The dynamics (2.17, 19) are of course fully determined by the choice of $F''(\xi)$, which leaves $F(\xi)$ undetermined by $A + B\xi$; the terms containing the constants A, B cancel in (2.17, 19). Actually, θ is itself arbitrary to within a constant, so that $F(\xi)$ is undetermined by $A + B\xi + C\xi^2$. We shall, however, adopt the convention of prescribing $F(\xi)$.

and

$$H \frac{\partial T}{\partial t} + J(\psi, T) - \frac{1}{6} Q \left(\frac{H}{y} \right)^3 \frac{\partial T}{\partial x} = 0. \tag{2.25}$$

Eqs. (2.24, 25) are perhaps the simplest dynamical equations that incorporate the effects of baroclinicity and bottom relief.

The choice

$$F(\xi) = \begin{cases} \frac{1}{2} g' \xi^2, & \xi > 0 \\ 0 & \xi < 0 \end{cases} \tag{2.26}$$

with $h(x, y, t)$ defined by

$$S(x, y, t) = \frac{h(x, y, t)}{y} \tag{2.27}$$

corresponds to the conventional two-layer model, in which an upper layer of depth $h(x, y, t)$ and uniform temperature g' overlies a layer of zero temperature. (The g' notation anticipates the dimensional form.) That is, with (2.26), (2.17, 19) reduce to the conventional two-layer equations,

$$J \left(\psi, \frac{y}{H} \right) + J \left(\frac{1}{H}, \frac{1}{2} g' h^2 \right) = 0 \tag{2.28}$$

and

$$\frac{\partial h}{\partial t} + J \left(\psi, \frac{h}{H} \right) + J \left(\frac{1}{2} g' h^2, \frac{1}{y} \left(1 - \frac{h}{H} \right) \right) = 0 \tag{2.29}$$

for $0 < h(x, y, t) < H$. For $h < 0$ or $h > H$ (2.17, 19) reduce correctly to the homogeneous-fluid limit, in which the upper or lower layer fills the water column. For an independent derivation of (2.28, 29), see for example Salmon (1992).

Ford (1992) has considered the corresponding case of a layer with uniform potential vorticity $y \theta_z = Q$ and thickness h overlying a layer of uniformly zero temperature, with no temperature jump between the layers, corresponding to (2.4) and the choice

$$F(\xi) = \begin{cases} \frac{1}{6} Q \xi^3, & \xi > 0 \\ 0 & \xi < 0 . \end{cases} \tag{2.30}$$

This temperature structure may resemble the observed ocean more closely than the conventional homogeneous-temperature-layers case. For $0 < h < H$, Ford's equations are

$$J \left(\psi, \frac{y}{H} \right) + J \left(\frac{1}{H}, \frac{1}{6} Q \frac{h^3}{y} \right) = 0 \tag{2.31}$$

and

$$\frac{\partial h}{\partial t} + J\left(\psi, \frac{h}{H}\right) + J\left(\frac{1}{6}Q\frac{h^3}{y}, \frac{1}{y}\left(1 - \frac{h}{H}\right)\right) = 0. \tag{2.32}$$

Although analytically simple, the two-layer dynamics (2.28, 29) or (2.31, 32) are an awkward basis for numerical experiments, because it is difficult to follow the outcropping line, $h = 0$, of the meniscus between the layers. From the perspective of (2.4), this difficulty occurs only because the choices (2.26) or (2.30) correspond to $F(\xi)$ with discontinuous derivatives. However, we can completely overcome this difficulty by replacing (2.26) and (2.30) by

$$F(\xi) = \frac{1}{2}g'\xi^2\Lambda(\xi) \tag{2.33}$$

and

$$F(\xi) = \frac{1}{6}Q\xi^3\Lambda(\xi) \tag{2.34}$$

respectively, where

$$\Lambda(\xi) = \frac{1}{2}\left\{\tanh\left(\frac{\xi}{d}\right) + 1\right\} \tag{2.35}$$

is a smooth approximation to the Heaviside function, which increases from zero to unity in an interval of order d centered on $\xi = 0$. The resulting forms of (2.17, 19) approach (2.28, 29) and (2.31, 32) as $d \to 0$. However, when $d > 0$, there is no need to follow the outcropping meniscus explicitly, because the temperature (2.4) and its derivatives are everywhere continuous. That is, when $d > 0$ is small, and $0 < h < H$, then $h(x, y, t)$ defined by (2.27) retains its physical interpretation as the depth of the upper, uniform-temperature or uniform-potential-vorticity "layer," but the line $h = 0$ is a line of large but *finite* surface temperature gradient. The case $d > 0$ is also more realistic, because the observed main thermocline is actually several hundred meters thick.

In this paper, we analyze analytical and numerical solutions of the generalized two-layer equations (GTLE), (2.17, 19), with forcing and dissipation terms added, for several choices of the profile function $F(\xi)$. For any $F(\xi)$, the GTLE contain the two dependent variables $\psi(x, y, t)$ and $S(x, y, t)$, which do not depend on the vertical coordinate z. This reduction in the number of the *independent* variables is the really significant simplification of the theory, and it is the basis for the general solution of the ideal GTLE in Section 3. Other methods of reduction besides the ansatz (2.4) are possible (see e.g. Salmon and Hollerbach, 1991), and at least one method yields a system with *four* vertical degrees of freedom: Ford (1992) has considered the case of

two immiscible layers of uniform potential vorticity, corresponding to the temperature structure

$$
\theta = \begin{cases} Q_1 \dfrac{z}{y} + T_1(x, y, t) & z > -h(x, y, t) \\ \\ Q_2 \dfrac{z}{y} + T_2(x, y, t) & z < -h(x, y, t). \end{cases}
\tag{2.36}
$$

With the ansatz (2.36), (2.1–2) lead, without further approximation, to rather complicated, coupled equations for the *four* dependent variables $\psi(x, y, t)$, $h(x, y, t)$, $T_1(x, y, t)$ and $T_2(x, y, t)$. The dynamics (2.28, 29) and (2.31, 32) emerge as very special cases. For now, however, the challenge posed by the GTLE (2.17, 19) seems sufficient, and the evidence suggests that the generalized two-layer equations might explain many observed features of the general ocean circulation.

3. General solution of the ideal equations

We begin our analysis of the GTLE by writing down their general, steady solution. Nothing better illustrates the power of the method of characteristics. Let $\partial S / \partial t = 0$ and rewrite (2.17, 19) in the form of potential vorticity equations,

$$
J(\psi, q_1) + c(q_1, q_2) J(q_1, y) = 0
\tag{3.1}
$$

and

$$
J(\psi, q_2) + c(q_1, q_2) J(q_2, y) + c_H(q_1, q_2) J(q_2, H) = 0.
\tag{3.2}
$$

Here

$$
q_1 \equiv S \qquad \text{and} \qquad q_2 \equiv S - \frac{H}{y}
\tag{3.3}
$$

are the "potential vorticities of the top and bottom layers,"

$$
c = 2F(q_1) - 2F(q_2) - (q_1 - q_2)[F'(q_1) + F'(q_2)]
\tag{3.4}
$$

is the Rossby phase speed defined by (2.20), and

$$
c_H \equiv F'(q_1) - F'(q_2) - (q_1 - q_2)F''(q_2).
\tag{3.5}
$$

Strictly speaking, q_1 and q_2 are the potential vorticities only in the special case (2.26) of the conventional two-layer equations, when, again defining $h \equiv yS$, (3.3) reduce to the familiar forms $q_1 = h/y$ and $q_2 = (h - H)/y$. However, these quantities are also closely related to the values of the potential vorticity $y\theta_z$ at $z = 0$, $-H$ (namely $F'''(S)$

and $F'''(S - H/y)$ respectively), and it is easy to show that (3.1–2) express the constancy of $y\theta_z$ on particles moving along these boundaries.

Now, (3.1–2) are also characteristic equations in which the q_i play the role of Riemann invariants. Following Salmon (1992) and Ford (1992), there are two cases to consider. In the first case,

$$\frac{\partial(q_1, q_2)}{\partial(x, y)} = 0 \tag{3.6}$$

and lines of constant q_1, q_2, and H/y all coincide. Then letting

$$q_1 = G(\alpha), \qquad \text{where} \qquad \alpha \equiv H/y \tag{3.7}$$

so that

$$q_2 = G(\alpha) - \alpha, \tag{3.8}$$

we regard α and y as new independent variables, and rewrite the characteristic equations (3.1–2) as equations for $G(\alpha)$ and $\psi(\alpha, y)$, viz.

$$G'(\alpha)\left[-\frac{\partial \psi}{\partial y} + c\right] = 0 \tag{3.9}$$

and

$$[G'(\alpha) - 1]\left[-\frac{\partial \psi}{\partial y} + c + \alpha c_H\right] = 0. \tag{3.10}$$

There are now two possibilities. Either

$$G'(\alpha) = 0 \qquad \text{and} \qquad -\frac{\partial \psi}{\partial y} + c + \alpha c_H = 0 \tag{3.11}$$

or

$$G'(\alpha) = 1 \qquad \text{and} \qquad -\frac{\partial \psi}{\partial y} + c = 0. \tag{3.12}$$

By easy steps, these two alternatives lead to the two solutions

$$q_1 \equiv S = Q_1$$

$$\psi = \left[2yF(Q_1) - 2yF\left(Q_1 - \frac{H}{y}\right) - 2HF'\left(Q_1 - \frac{H}{y}\right)\right.$$
$$\left. - \frac{H^2}{y}F''\left(Q_1 - \frac{H}{y}\right)\right] + R_1\left(\frac{H}{y}\right) \tag{3.13}$$

and

$$q_2 \equiv S - \frac{H}{y} = Q_2$$

$$\psi = \left[2yF\left(Q_2 + \frac{H}{y}\right) - 2yF(Q_2) - HF'\left(Q_2 + \frac{H}{y}\right) \right. \tag{3.14}$$

$$\left. - HF'(Q_2) \right] + R_2\left(\frac{H}{y}\right)$$

where the Q_i are arbitrary constants, and the R_i are arbitrary functions. The solutions (3.13) and (3.14) correspond to flows in which the upper- and lower-layer potential vorticities are (respectively) uniform.

In the second case,

$$\frac{\partial(q_1, q_2)}{\partial(x, y)} \neq 0 \tag{3.15}$$

and we can take q_1 and q_2 as new independent variables. In these coordinates, the characteristic equations (3.1–2) take the forms

$$\frac{\partial \psi}{\partial q_2} - c \frac{\partial y}{\partial q_2} = 0 \tag{3.16}$$

and

$$\frac{\partial \psi}{\partial q_1} - c \frac{\partial y}{\partial q_1} - c_H \frac{\partial H}{\partial q_1} = 0. \tag{3.17}$$

Noting that $H = y(q_1 - q_2)$, and eliminating ψ between (3.16) and (3.17), we eventually obtain

$$\frac{\partial^2}{\partial q_1 \partial q_2} [c_H y] = 0 \tag{3.18}$$

with solution

$$y = \frac{1}{c_H(q_1, q_2)} \{\Omega'_1(q_1) + \Omega'_2(q_2)\} \tag{3.19}$$

where Ω_1 and Ω_2 are arbitrary functions. By use of (3.3), (3.19) determines S implicitly. Then solving (3.16–17) for $\psi(\alpha, y)$, we obtain

$$\psi = \frac{c}{c_H} [\Omega'_1(q_1) + \Omega'_2(q_2)] + (q_1 - q_2)\Omega'_1(q_1) - \Omega_1(q_1) - \Omega_2(q_2). \tag{3.20}$$

In overall summary, the general steady solution of the ideal GTLE is (3.13), or (3.14), or (3.19–20). Solutions of the form (3.19–20) are of course generally multivalued; that is, depending on the functions $\Omega_1(\ )$ and $\Omega_2(\ )$, (3.19) could be satisfied by several values of S.

For the choices (2.26) and (2.30) of the profile function $F(\ )$, the general solution corresponds, respectively, to that found by Salmon (1992) and Ford (1992). Considering the standard case (2.26) of uniform-temperature layers, S92 suggested that the flow along western continental slopes can be viewed as a composite of uniform-potential-vorticity solutions of the types (3.13) and (3.14), separated by a dissipative inner region required by matching. More specifically, the Gulf Stream corresponds to a region of uniform lower-layer potential vorticity, which is matched to an offshore region of uniform upper-layer potential vorticity by a frictional inner region containing a strong southward flow. Both the northward transport of the Gulf Stream and the southward transport in this seaward countercurrent are significantly stronger than in the corresponding solution for homogeneous (i.e. single-layer) flow. Thus, topography and baroclinicity cause a large recirculation on the continental slope.

These results extend easily to the GTLE. That is, following the same steps as in S92, we may show that the uniform-potential-vorticity solutions (3.13–14) can be matched only along H/y-lines at which ψ must jump but S may not; that the jump in ψ is caused by a jump in the JEBAR[4] torque, $J(\gamma, 1/H)$, in (2.17); and that the transition occurs in a frictional internal boundary layer with a significant southward transport. This generalization is significant because, although the conventional two-layer equations are difficult to solve numerically, the GTLE are not, and their numerical solution may help to determine whether solutions like those suggested by S92 actually occur as a part of fully self-consistent, whole-basin solutions. In particular, it is not necessary to regard the GTLE as an approximation to the conventional two-layer equations, because the GTLE are important in their own right, and, seemingly, everything that can be proved for the conventional equations can be proved directly for the GTLE.

Of course, full-basin numerical solutions require wind- and thermal-forcing, and, as already remarked, (2.1–2) can satisfy boundary conditions of no-net-transport at coastal boundaries only if friction terms are also added to (2.1). In the following section, we show how dissipation and forcing can be added to the GTLE without cancelling their other advantages. Although the general, dissipative, planetary geostrophic equations (4.1–2) remain well-posed at the equator, $y = 0$, (where Darcy's law replaces geostrophic balance) the prescribed temperature (2.4) has an undesirable singularity there, and we also propose a strategy for removing this singularity.

---

4. "Joint Effect of Baroclinicity and Topography"

4. Forcing, dissipation, and the equator

Consider now the *nonconservative* form of the planetary geostrophic equations,

$$-fv = -\phi_x - \epsilon u - fv_E$$
$$fu = -\phi_y - \epsilon v + fu_E$$
$$0 = -\phi_z + \theta$$
$$u_x + v_y + w_z = 0$$

(4.1)

and

$$\theta_t + u\theta_x + v\theta_y + w\theta_z = \kappa\nabla_3^2\theta \tag{4.2}$$

with the forcing and dissipation terms suggested by Salmon (1986, 1990, 1992). Here $\nabla_3 \equiv (\partial_x, \partial_y, \partial_z)$, ϵ is a coefficient of Rayleigh friction in the horizontal direction, and κ is the diffusion coefficient for temperature. The prescribed functions

$$(u_E, v_E) \equiv \mathbf{u}_E(x, y, z) \tag{4.3}$$

represent horizontal body forces that model the input of wind momentum near the ocean surface; except near $y = 0$, we can regard $\mathbf{u}_E$ as the Ekman-layer contribution to the horizontal velocity $\mathbf{u}$. As shown in the previous papers, (4.1–2) are well-posed with respect to boundary conditions of no-normal-flow and prescribed temperature (or temperature flux), provided that the ocean depth $H(x, y)$ vanishes smoothly at the coastline. If vertical sidewall boundaries are present, then the vertical momentum equation (4.1c) must also contain a Rayleigh friction term.

The case for (4.1–2) has been made in the previous papers; see especially Salmon (1992). Briefly, Rayleigh friction is *allowed* because (4.1) omits the advection of momentum. Rayleigh friction is *desirable* because it leads to a relatively simple (and numerically resolvable) boundary-layer structure. The simple friction *requires* wind-forcing to be the body-force represented by (4.3) rather than a prescribed surface stress. However, *temperature* diffusion is required, because temperature *advection* has been retained.

To see that (4.1–2) are well-posed, suppose that all the variables are known at some time t. Then the temperature equation (4.2) and temperature boundary conditions determine θ at the later time $t + dt$. To continue, we must determine the velocity field at $t + dt$. This velocity field is instantaneously determined by θ, the linear equations (4.1), and the no-normal-flow boundary conditions, as follows. First note that the continuity equation (4.1d) and the top- and bottom-boundary conditions (2.9) and (2.10) imply (2.13) and (2.14) as before. Then substitute the vertical integral of the horizontal momentum equations (4.1a, b) into (2.14) and cross-differentiate to remove the pressure. The result is

$$J\left(\psi, \frac{y}{H}\right) + J\left(\frac{1}{H}, \gamma\right) = W(x, y) - \nabla \cdot \left(\frac{\epsilon}{H}\nabla\psi\right) \tag{4.4}$$

where

$$\gamma(x, y) \equiv - \int_{-H}^{0} z\theta \, dz, \tag{4.5}$$

as before;

$$W(x, y) \equiv \nabla \cdot (y\bar{\mathbf{u}}_E) \tag{4.6}$$

is the wind-stress curl, and

$$\bar{\mathbf{u}}_E \equiv \frac{1}{H} \int_{-H}^{0} \mathbf{u}_E \, dz \tag{4.7}$$

i.e. the overbar denotes the vertical average.

For given θ, ψ is uniquely determined by the elliptic equation (4.4) and the boundary condition $\psi = 0$ at coastlines. With ψ determined, the velocity field is given by

$$\mathbf{u} \equiv (u, v) = \frac{1}{H} \mathbf{k} \times \nabla\psi + \mathbf{u}' \tag{4.8}$$

and

$$w = \int_{z}^{0} \nabla \cdot \mathbf{u} \, dz' \tag{4.9}$$

where $\mathbf{u}'$, the departure of the horizontal velocity from its vertical average, is determined by

$$\begin{aligned}
\frac{\partial u'}{\partial z} &= \frac{1}{y^2 + \epsilon^2} \left[-y\theta_y - \epsilon\theta_x + y \left(y \frac{\partial u_E}{\partial z} - \epsilon \frac{\partial v_E}{\partial z} \right) \right] \\
\frac{\partial v'}{\partial z} &= \frac{1}{y^2 + \epsilon^2} \left[y\theta_x - \epsilon\theta_y + y \left(y \frac{\partial v_E}{\partial z} + \epsilon \frac{\partial u_E}{\partial z} \right) \right]
\end{aligned} \tag{4.10}$$

and

$$\int_{-H}^{0} \mathbf{u}' \, dz = 0. \tag{4.11}$$

As in the previous papers, we are interested in the case of very small ϵ and κ. If ϵ is small, and if, as in the previous papers, the model ocean excludes the equator at $y = 0$, then we can consistently replace (4.10) by the simpler equations

$$\begin{aligned}
\frac{\partial u'}{\partial z} &= -\frac{1}{y} \theta_y - \frac{\epsilon}{y^2} \theta_x + \frac{\partial u_E}{\partial z} \\
\frac{\partial v'}{\partial z} &= \frac{1}{y} \theta_x - \frac{\epsilon}{y^2} \theta_y + \frac{\partial v_E}{\partial z}.
\end{aligned} \tag{4.12}$$

If, as in this paper, the model ocean includes the equator, we must use the more general form (4.10). However, if ϵ is small, (4.10) and (4.12) differ only in an equatorial region of width ϵ.

Eq. (4.4) is the generalization of Stommel's (1948) vorticity equation to include the bottom torque. The fact that the three-dimensional velocity is determined, through (4.4), by the temperature field $\theta(x, y, z)$ is an instance of the *invertibility principle* (Hoskins *et al.*, 1985), which states that the potential vorticity field (and, typically, some ancillary information about the temperature field) determines the velocity field. In the case of the planetary geostrophic equations (4.1–2), the potential vorticity $y\theta_z$ and the temperature θ are very closely related, but the invertibility principle applies most simply to θ; for a given potential vorticity field, one would also need to know the temperature at one level (e.g. at the ocean surface or bottom) to obtain the velocity field (u, v, w).

The temperature ansatz (2.4) contains a singularity at the equator. We therefore modify (2.4), assuming instead that

$$\theta = F''\left(\frac{z}{Y} + S(x, y, t)\right) \tag{4.13}$$

where

$$Y \equiv \sqrt{y^2 + \delta^2}, \tag{4.14}$$

δ is a prescribed constant, and F'' is an arbitrary function, as before. Outside an equatorial zone of width δ, the new ansatz (4.13) agrees with the old ansatz (2.4) and shares its special status. Near the equator, (4.13) has no special status but contains no singularity. I stress that the *definition* (4.14) is *not* an assumption about the dependence of the Coriolis parameter, y, on location; nor should the Y defined by (4.14) be viewed as a new coordinate. The ansatz (4.13–14) does impose the reasonable restriction that, *apart from the effect of S*, the temperature θ be symmetric about the equator. However, $S(x, y, t)$ need have no symmetry of any kind, and thus, although we consider below only completely symmetric temperatures and circulations, cross-equatorial symmetry is not required by (4.13).

If the temperature takes the form (4.13), then (4.5) becomes

$$\gamma = Y^2 F(S) - Y^2 F\left(S - \frac{H}{Y}\right) - HY F'\left(S - \frac{H}{Y}\right). \tag{4.15}$$

When W, ϵ and δ all vanish, (4.4, 15) reduce to (2.17–18).

To obtain the generalization of the S-equation (2.19), we substitute our basic temperature ansatz (4.13) into (4.10), solve (4.10–11) for $\mathbf{u}$, and then substitute the temperature (4.13) and velocity components (4.8–9) into the temperature equation (4.2). The resulting (rather complicated) equation *cannot* be satisfied at every (x, y, z)

for *any* $\psi(x, y, t)$ or $S(x, y, t)$. This is expected, because the ansatz (2.4) bore a special relationship to the ideal-fluid equations (2.1–2), and this relationship is destroyed by the forcing and dissipation terms, and by the modification required to remove the equatorial singularity. When forcing and dissipation are present (or when $\delta \neq 0$), only a single vertical moment of the temperature equation (4.2) can be required to vanish at every (x, y). That is, we must then *project* the forcing and dissipation onto the evolution equation for S, thereby admitting nonconservative effects only to an extent compatible with maintaining the prescribed structure (4.13) of the model. The significant point is that this structure is maintained exactly where nonconservative effects are unimportant, and outside the equatorial region of width δ. That is, apart from forcing, the solutions of the resulting equations are also solutions of the full three-dimensional equations (4.1–2), except (assuming ϵ, κ and δ are small) in thin dissipative layers and near the equator. In the dissipative and equatorial regions, the equations have the status of an ordinary Galerkin approximation.[5]

We will require that the vertical integral of the temperature equation (4.2) vanish, i.e.

$$\frac{\partial}{\partial t} \int_{-H}^{0} \theta \, dz + \nabla \cdot \left[\int_{-H}^{0} \mathbf{u}\theta \, dz \right] = \nabla \cdot \left[\int_{-H}^{0} \kappa \nabla \theta \, dz \right] + Q \qquad (4.16)$$

where Q represents the surface heat flux (and we have assumed no heat flux into the ocean bottom). By our fundamental ansatz (4.13), the first term in (4.16) takes the form

$$H \frac{\partial \bar{\theta}}{\partial t} = \mu \frac{\partial S}{\partial t} \qquad (4.17)$$

where

$$\bar{\theta} \equiv \frac{1}{H} \int_{-H}^{0} \theta \, dz = \frac{Y}{H} (F'_T - F'_B) \qquad (4.18)$$

and

$$\mu \equiv Y(\theta_T - \theta_B) = Y(F''_T - F''_B) \qquad (4.19)$$

and we have introduced a short-hand notation,

$$F_T \equiv F(S), \qquad F'_T \equiv F'(S), \qquad F''_B \equiv F''\left(S - \frac{H}{Y}\right), \text{ etc.} \qquad (4.20)$$

in which the subscripts T and B denote *top* and *bottom*, respectively.

---

5. More precisely, our projection corresponds to the "method of weighted residuals" because the projection—a vertical average of the temperature equation—is unrelated to the temperature representation (4.13).

To develop the second term in (4.16), we first solve (4.8, 10–11) for the horizontal velocity components,

$$u = -\frac{1}{H}\psi_y + \frac{1}{y^2 + \epsilon^2}\{-yG[\theta_y] - \epsilon G[\theta_x] + y^2 u'_E - \epsilon y v'_E\} \tag{4.21}$$

and

$$v = \frac{1}{H}\psi_x + \frac{1}{y^2 + \epsilon^2}\{yG[\theta_x] - \epsilon G[\theta_y] + y^2 v'_E + \epsilon y u'_E\}. \tag{4.22}$$

Here, $G[r(z)]$ is defined as the solution to

$$\frac{du}{dz} = r(z), \qquad \int_{-H}^{0} u\, dz = 0 \tag{4.23}$$

namely,

$$G[r(z)] \equiv \int_{-H}^{z} r(z')\, dz' + \frac{1}{H}\int_{-H}^{0} z' r(z')\, dz' \tag{4.24}$$

and u'_E is the departure of the Ekman velocity from its vertical average. The first term on the right-hand sides of (4.21–22) represents the vertically-averaged horizontal velocity $\bar{u}$; the remaining terms represent u'. The corresponding contributions to the second term in (4.16) are

$$\nabla \cdot \left[\int_{-H}^{0} \bar{u}\theta\, dz\right] = \nabla \cdot (\bar{u}H\theta) = J(\psi, \bar{\theta}) \tag{4.25}$$

and

$$\nabla \cdot \left[\int_{-H}^{0} u'\theta\, dz\right] = \frac{\partial}{\partial x}\left[\frac{1}{y^2 + \epsilon^2}(-yG^y - \epsilon G^x)\right]$$

$$+ \frac{\partial}{\partial y}\left[\frac{1}{y^2 + \epsilon^2}(yG^x - \epsilon G^y)\right] \tag{4.26}$$

$$+ \nabla \cdot \left[\frac{y^2}{y^2 + \epsilon^2}\int_{-H}^{0}\theta u'_E\, dz\right] - \text{curl}\left[\frac{\epsilon y}{y^2 + \epsilon^2}\int_{-H}^{0}\theta u'_E\, dz\right]$$

where, again using (4.13),

$$(G^x, G^y) \equiv \int_{-H}^{0}\theta G[\nabla\theta]\, dz = Y\int_{-H}^{0}\left(\frac{\partial S}{\partial x}, \frac{\partial S}{\partial y} - \frac{zy}{Y^3}\right)(\theta - \bar{\theta})^2\, dz. \tag{4.27}$$

We simplify the u'_E-terms in (4.26) by assuming that u_E is nonzero only within a thin layer near $z = 0$ in which the temperature is approximately equal to its surface value;

then

$$\int_{-H}^{0} \theta u'_E \, dz = [\theta(x, y, 0) - \bar{\theta}] H \bar{u}_E. \tag{4.28}$$

Finally, the diffusion term in (4.16) takes the form

$$\nabla \cdot \left[\kappa \int_{-H}^{0} \nabla \theta \, dz \right] = \nabla \cdot [\kappa(\mu \nabla S + \alpha \mathbf{j})] \tag{4.29}$$

where $\mathbf{j}$ is the northward unit vector, μ is given by (4.19), and

$$\alpha \equiv -\frac{y}{Y^2} \int_{-H}^{0} z \theta_z \, dz = \frac{yH}{Y^2} (\bar{\theta} - \theta_B) = \frac{y}{Y} \left(F'_T - F'_B - \frac{H}{Y} F''_B \right). \tag{4.30}$$

We substitute all these results back into (4.16) and group the terms so that the resulting equation resembles a weighted average of the characteristic equations (3.1–3) for potential vorticity (to which it must clearly reduce in the ideal-fluid limit, $Q \equiv \mathbf{u}_E \equiv 0 = \epsilon = \delta = \kappa$). A year of experimentation has shown that this form of the S-equation is a particularly stable basis for numerical solution. The algebra is very tedious but straightforward. The final result is

$$W_T \left\{ H \frac{\partial S}{\partial t} + J(\psi, S) + \tilde{c} J(S, y) - \mathbf{v}_T \cdot \nabla S \right\}$$

$$+ W_B \left\{ H \frac{\partial}{\partial t} \left(S - \frac{H}{Y} \right) + J \left(\psi, S - \frac{H}{Y} \right) + \tilde{c} J \left(S - \frac{H}{Y}, y \right) \right.$$

$$\left. + \tilde{c}_H J \left(S - \frac{H}{Y}, H \right) - \mathbf{v}_B \cdot \nabla \left(S - \frac{H}{Y} \right) \right\} + c_e \frac{\partial S}{\partial x} \tag{4.31}$$

$$= \nabla \cdot [\epsilon(D \nabla S + E \mathbf{j})] + \nabla \cdot [\kappa(\mu \nabla S + \alpha \mathbf{j})] + Q(x, y) + W_s(x, y)$$

Here,

$$W_T \equiv \frac{Y}{H} (\theta_T - \bar{\theta}), \qquad W_B \equiv \frac{Y}{H} (\bar{\theta} - \theta_B) \tag{4.32}$$

are the weight factors,

$$\tilde{c} \equiv \frac{y^2}{Y^2(y^2 + \epsilon^2)} \int_{-H}^{0} z(z + H) \theta_z \, dz = \frac{y^2}{(y^2 + \epsilon^2)} \left[2(F_T - F_B) - \frac{H}{Y} (F'_T + F'_B) \right] \tag{4.33}$$

corresponds to the Rossby wave speed (3.4),

$$\tilde{c}_H \equiv \frac{yH}{y^2 + \epsilon^2} (\bar{\theta} - \theta_B) \tag{4.34}$$

corresponds to (3.5), and

$$c_e \equiv \frac{(\delta^2 \epsilon^2 + 2\epsilon^2 y^2 - \delta^2 y^2)}{Y(y^2 + \epsilon^2)^2} \int_{-H}^{0} (\theta - \bar{\theta})^2 \, dz \qquad (4.35)$$

is small except near the equator, where it contributes an eastward propagation tendency to S. The terms containing

$$\mathbf{v}_B \equiv \frac{yH}{y^2 + \epsilon^2} (y\bar{u}_E - \epsilon\bar{v}_E, y\bar{v}_E + \epsilon\bar{u}_E) \qquad (4.36)$$

and

$$\mathbf{v}_T \equiv (1 - F_T'''/W_T)\mathbf{v}_B \qquad (4.37)$$

now carry the influence of $\mathbf{u}_E'$ on the temperature field. The diffusion coefficients on the right-hand side of (4.31) are defined by

$$D \equiv \frac{Y}{y^2 + \epsilon^2} \int_{-H}^{0} (\theta - \bar{\theta})^2 \, dz = \frac{Y^2}{y^2 + \epsilon^2} [M(S) - M(S - H/Y)] - \frac{YH}{y^2 + \epsilon^2} \bar{\theta}^2 \quad (4.38)$$

and

$$E \equiv - \frac{y}{Y^2(y^2 + \epsilon^2)} \int_{-H}^{0} z(\theta - \bar{\theta})^2 \, dz$$

$$= \frac{y}{y^2 + \epsilon^2} \left\{ (N_B - N_T) + S(M_T - M_B) \right.$$

$$\left. + (F_T' - F_B')\left(\frac{3}{2} F_B' + \frac{1}{2} F_T' + 2\frac{Y}{H}(F_B - F_T)\right) \right\} \qquad (4.39)$$

where

$$M(\xi) \equiv \int_{0}^{\xi} F''(\eta)^2 \, d\eta, \qquad N(\xi) \equiv \int_{0}^{\xi} \eta F''(\eta)^2 \, d\eta \qquad (4.40)$$

and μ and α are defined by (4.19) and (4.30). Again, Q is the surface heat flux, and the baroclinic wind forcing is defined by

$$W_s(x, y) \equiv (\theta_T - \bar{\theta})\left[-\nabla \cdot \left(\frac{y^2 H \bar{u}_E}{y^2 + \epsilon^2} \right) + curl \left(\frac{\epsilon y H \bar{u}_E}{y^2 + \epsilon^2} \right) \right] \qquad (4.41)$$

where *curl* denotes the vertical component of the curl $(\mathbf{k} \cdot \nabla \times)$. In the limit of no forcing and dissipation, and $\delta \to 0$, we see that $\tilde{c} \to c$, $\tilde{c}_H \to c_H$, $c_e \to 0$, and the right-hand side of (4.31) vanishes along with $\mathbf{v}_T$ and $\mathbf{v}_B$. In this limit, (4.31) reduces, as it must, to a weighted average of the characteristic equations (3.1–3). Note from

(4.32) that the "thinnest" layer receives the most weight in (4.31); the potential vorticity of the "thickest" layer is more strongly controlled by the depth-averaged equation, (4.4).

Eqs. (4.4) and (4.31) are the nonconservative form of the GTLE, the generalizations of (2.17, 19) to include forcing and dissipation and to accommodate an equator. We see that the forcing and dissipation terms in (4.1–2) lead to forcing and diffusion terms in (4.4, 31), and that the δ-modification (4.13) removes the singularity in (2.19) at $y = 0$. Indeed, whereas c and c_H are both infinite at $y = 0$, $\tilde{c}$ and $\tilde{c}_H$ both vanish there. The Rayleigh friction ϵ and the temperature diffusion κ *both* contribute diffusion terms to (4.31), but a close analysis shows that the κ-terms are indispensable, essentially because D vanishes faster than μ as $H \to 0$.

As a check on (4.4) and (4.31), we write them out for the choice (2.26) of profile function corresponding to the conventional case of two homogeneous layers. In the cases where S and $S - H/Y$ have the same sign, one of the layers fills the whole water column, and the JEBAR term in (4.4) vanishes, as do all the terms in (4.31). In the case where $S > 0$ and $S - H/Y < 0$, the depth $h = YS$ of the upper layer is between 0 and H. By carefully evaluating all terms, we find that (4.4) and (4.31) reduce to

$$J\left(\psi, \frac{y}{H}\right) + J\left(\frac{1}{H}, \frac{1}{2}g'h^2\right) = \nabla \cdot (y\bar{\mathbf{u}}_E) - \nabla \cdot \left(\frac{\epsilon}{H}\nabla\psi\right) \tag{4.42}$$

and

$$\frac{\partial h}{\partial t} + J\left(\psi, \frac{h}{H}\right) + J\left(g'h, \frac{yh}{y^2 + \epsilon^2}\left(1 - \frac{h}{H}\right)\right) = \nabla \cdot \left[\epsilon \frac{g'h}{y^2 + \epsilon^2}\left(1 - \frac{h}{H}\right)\nabla h\right]$$
$$+ \kappa\nabla^2 h + Q/g' - \nabla \cdot \left[\frac{y^2(H - h)}{y^2 + \epsilon^2}\bar{\mathbf{u}}_E\right] + \operatorname{curl}\left[\frac{\epsilon y(H - h)}{y^2 + \epsilon^2}\bar{\mathbf{u}}_E\right]. \tag{4.43}$$

Eqs. (4.42–43) are the same equations one would obtain by assuming, *a priori*, the existence of two homogeneous, immiscible layers with Rayleigh friction ϵ and forcing distributed uniformly with depth in the upper layer of thickness h. This limit provides an independent check on the nonconservative form of the GTLE and thus on the choice of vertical moment (4.16).

Interestingly, the conventional two-layer equations (4.42–43) are well-posed with respect to boundary conditions of no-normal-flow at *vertical* sidewalls. The boundary conditions $\psi = 0$ and

$$g'\frac{\partial h}{\partial s} + g'\frac{\epsilon}{y}\frac{\partial h}{\partial n} = y\frac{H}{h}\bar{\mathbf{u}}_E \cdot \mathbf{n} - \epsilon\frac{H}{h}\bar{\mathbf{u}}_E \cdot \mathbf{s} \tag{4.44}$$

(where $\mathbf{n}$ is the outward unit normal, and $\mathbf{s}$ the counterclockwise-pointing unit tangent) guarantee that the normal flow vanishes in both layers. In the GTLE, no

single boundary condition can make the flow vanish at all depths, but the Galerkin-type boundary condition

$$\int_{-H}^{0} \theta \mathbf{u} \, dz \cdot \mathbf{n} = 0 \tag{4.45}$$

reduces to (4.44) for the profile function (2.26) corresponding to two conventional layers.

In this paper, we consider only geometries with vanishing depth, $H = 0$, at coastlines. Then, if $\psi = 0$ at the coastline, the normal advective flux is automatically zero there, but the requirement that the normal *diffusive* flux also vanish imposes the boundary condition

$$\nabla S \cdot \mathbf{n} = 0. \tag{4.46}$$

In the following section, we briefly review some of the previous work with two-layer *flat-bottom* ocean models. Then in Section 6, we turn to numerical solutions of the GTLE, (4.4, 31) in oceans with nonuniform depth. Because (4.4, 31) are very much more complicated than (2.17, 19), there is now no hope of general analytical solution. However, it does at least seem likely that solutions of the GTLE are qualitatively insensitive to the precise form of the forcing and dissipation, so that one might replace the nonconservative terms in (4.31) by simpler terms of the same general character without losing any of the essential physics. Indeed, much of the interpretation in Sections 5 and 6 rests on the tacit assumption that the precise forms of the nonconservative terms are irrelevant. In this initial study, I nevertheless decided to follow the safer course of using nonconservative terms derived in the straightforward but somewhat laborious manner described above.

5. Remarks on the flat-bottom case

Although we consider only cases in which the ocean depth vanishes at the coastlines, most previous workers have considered model oceans with uniform depth. We therefore begin with a brief survey of the flat-bottom case.

If $H \equiv 1$, the ψ-equation (4.4) reduces to Stommel's equation,

$$\frac{\partial \psi}{\partial x} = W(x, y) - \epsilon \nabla^2 \psi \tag{5.1}$$

and ψ is determined solely by the wind-stress curl, W, and is unaffected by θ. We may then regard $\psi(x, y)$ as prescribed, in the same sense as $W(x, y)$. Then (4.31) becomes a *quasilinear* equation for S, which, in steady state, takes the form

$$J(\psi, S) + c\left(S, \frac{H}{y}\right) \frac{\partial S}{\partial x} = nonconserv. \tag{5.2}$$

where $\psi(x, y)$ is given, and the phase speed $c < 0$ is defined by (2.20–21). The left-hand side of (5.2) is the same as in (2.19), and the right-hand side of (5.2) contains all the nonconservative effects, i.e. all the terms by which (4.31) differs from (2.19). As suggested in Section 4, the forcing contribution to the right-hand side of (5.2) is important nearly everywhere, but the dissipation and equatorial modification terms are important only in localized regions. In the following discussion, we assume that much about the solution of (5.2) can be explained by the form of its left-hand side.

It is useful to regard (5.2) as an "advection/diffusion" equation for S in which the advecting velocity field is given, in parametric form, by

$$\frac{dx}{dt} = -\frac{\partial \psi}{\partial y} + c, \qquad \frac{dy}{dt} = \frac{\partial \psi}{\partial x} \tag{5.3}$$

and t is now the parameter. The equations (5.3) define characteristics in the (x, y) plane along which S changes according to

$$\frac{dS}{dt} = nonconserv. \tag{5.4}$$

and the right-hand side of (5.4) is the same as (5.2). For small ϵ and κ, the diffusion terms in (5.4) are negligible except in narrow "inner regions," so that the wind- and thermal forcing comprise the dominant contribution to the right-hand side of (5.4) almost everywhere. The *sign* of the diffusion terms is nevertheless essential; it determines the direction in which information flows along the characteristics (5.3). For diffusion terms like those in (4.31), information flows in the direction of increasing t as defined by (5.3) (i.e. westward, if $\psi \equiv 0$). These facts form the basis for a qualitative theory of (5.2).

Now, if c is S-independent, then the characteristics defined by (5.3) are also independent of S, i.e. unaffected by the size of the temperature field swept along them. Consulting (2.21), we see that the only profile function (2.4) that leads to S-independent c is that corresponding to the uniform-potential-vorticity case (2.22), for which (still assuming $H \equiv 1$)

$$c = -\frac{1}{6} Q \left(\frac{H}{y}\right)^3 \tag{5.5}$$

and the characteristic equations (5.3) integrate easily to

$$\psi - \frac{1}{12} Q \frac{H^3}{y^2} = const. \tag{5.6}$$

For this case, the horizontally-varying component of the temperature, S, is determined by an advection/diffusion eqution, (5.2), in which the advecting "velocity

field," (5.3), corresponds to a "streamfunction" given by the (entire) left-hand side of (5.6).

The qualitative nature of this solution is immediately clear. Suppose, for example, that the transport streamfunction has the form

$$\psi = \psi_0 \sin\left[\pi(y - y_0)\right]\{1 - x - e^{-x/\epsilon}\}, \qquad 0 < y - y_0 < 1 \qquad (5.7)$$

corresponding to the standard subtropical wind-gyre. The characteristic velocity (5.3) corresponding to (5.7) is then westward in the southern interior half-basin where *both* ψ and c contribute a westward component. This means that the temperature field S is carried westward along characteristics from the eastern boundary (while of course gradually increasing because of the forcing terms on the right-hand side of (5.4)). However, in the northern half-basin, the characteristic velocity can be eastward, if the wind amplitude ψ_0 is large enough to overcome c, whose size decreases rapidly with increasing y. In that case, S is swept eastward from the northern-most part of the western boundary, along characteristics that curve southward and then westward to intersect the western boundary again. At the bounding characteristic separating characteristics of western-boundary origin from those of eastern-boundary origin, S changes rapidly across characteristics, and diffusion becomes important. This region of rapid change is an internal boundary layer (but not a shock, because the characteristics (5.6) do not intersect).

The whole discussion of the preceding paragraph is of course closely analogous to that first advanced in the classic papers of Rhines and Young (1982), Young and Rhines (1982) and Ierley and Young (1983). These authors considered two-layer quasigeostrophic dynamics, in which the analog of c is *always* constant. (de Szoeke (1985) has extended the quasigeostrophic theory to the case of a gently sloping bottom, assuming that the dissipation in the lower layer is very small.) In general, however, i.e. for profile functions other than (2.22), c depends on S, the characteristics (5.3) depend on the value of S swept along them, and *shocks* occur where the characteristics intersect, i.e. where conflicting information about S flows to the same point from different directions.

Dewar (1987, 1991, 1992; see especially 1991) has emphasized the importance of shocks in the conventional two-layer model corresponding to the profile function (2.26–27), for which

$$c = -g'h(H - h)/y^2. \qquad (5.8)$$

For *general* profile functions, the magnitude of c increases with S in the range of typical interest (e.g. in the range $0 < h = yS < H/2$ for the conventional two-layer case). This means that the characteristic velocity (5.3) is more westward where the vertically-averaged temperature is greater, leading to the possibility of a shock separating colder water on the west (with eastward characteristic velocity) from warmer water on the east (with westward characteristic velocity). Such shocks replace the internal boundary layer of the uniform-potential-vorticity (or quasigeo-

strophic) case. The eastward increase of S (i.e. upper-layer depth in the conventional two-layer model) across the shock corresponds to a strong baroclinic current along the shock, northward near the ocean surface. A southward flow as depth exactly compensates this northward surface flow, because the depth-averaged flow (ψ) must, by (5.1), be smooth. These features were, I believe, first predicted in a theoretical analysis of the two-layer ocean by Kamenkovich and Reznik (1972), in which the shock coincided with the lower-layer outcrop line. In a very careful series of numerical experiments with the two-layer equations, Jarvis and Veronis (1994) have studied the structure of the shock, and the way in which the flow east of the shock is determined by conditions in the western boundary layer. They show that the shock need *not* coincide with the line of lower-layer outcrop in the two-layer model (a fact also evident from the perspective of the GTLE, where, for arbitrary temperature profile functions, even the definition of *outcrop* is quite fuzzy). The competition between ψ and c, leading to the formation of shocks separating regions controlled by boundary conditions on opposite sides of the ocean has also been discussed by other workers; see, for example, Cushman-Roisin (1984) and Luyten and Stommel (1986).

Although the *interior* flat-bottom equations are relatively simple, enabling a relatively simple interpretation of the interior solutions in terms of characteristics and shocks, the precise form of these solutions depends strongly on the values of S swept into the interior from the boundary layers along the coasts. As emphasized by Ierley and Young (1983) and Jarvis and Veronis (1994), these S-values are set by the complicated physics of the boundary layer, and the whole problem thus reduces to understanding the ways in which these boundary layers control the interior flow.

The whole character of the circulation problem changes if the ocean depth vanishes at coastlines. The GTLE are then more complicated, but *boundary* layers exert much less control (or are absent altogether), because the topography steers the characteristics *parallel* to the coastlines. The complicated "boundary physics" then occurs away from coastlines, on the continental slopes, in better agreement with observations. Of course, the variable topography makes the GTLE much harder to interpret. Although (5.2) keeps its same form, the JEBAR term in (4.4) lets the temperature field feed back on ψ, which is then no longer solely determined by the wind. The S-dependence of ψ means that (5.2) is no longer quasi-linear. This added complexity is the price of entertaining realistic topography, but there may also be a benefit: I strongly suspect that one reason for the slow progress in understanding flat-bottom ocean models may be the artificial sensitivity of the models to the unrealistic boundary layers at the vertical sidewalls. We now turn to numerical solutions of the GTLE without vertical sidewalls.

6. Numerical solutions of the GTLE

We begin by explaining the scaling of the fundamental nondimensional equations (4.1–2), which (4.4, 31) inherit. Suppose that (4.1–2) have been obtained from their dimensional counterparts by scaling: (x, y) by $L = 4000$ km (the ocean basin width), z

by H_0 = 4 km (a representative ocean depth), $\mathbf{u}$ and $\mathbf{u}_E$ by U (a representative horizontal velocity), w by H_0U/L, t by L/U, ϕ by f_0UL (where $f_0 = 10^{-4}$ sec^{-1}), and θ by f_0UL/H_0. We choose U = .2 km/day so that ULH_0 = 30 Sverdrups, the transport in the North Atlantic subtropical gyre; then the wind forcing is realistic if it produces a nondimensional transport streamfunction ψ with a maximum value of order unity. The *dimensional* buoyancy is related to potential density by

$$\theta = -\frac{g}{\rho_0} 10^{-3}\sigma_\theta \tag{6.1}$$

where g is gravity and ρ_0 = 1 gm cm^{-3}. Thus the observed range of θ is about 2 cm/sec^2. Dividing by .02 cm^2/sec, our buoyancy scale, we conclude that the nondimensional buoyancy range is about 100. This estimate affects the choice of temperature profile function.

We consider a model ocean on $0 < x < 1, 0 < y < 2$, with the bathymetry shown in Figure 1a. The ocean depth $H(x, y)$ vanishes at the western ($x = 0$), eastern ($x = 1$), and northern ($y = 2$) coastlines. (In all contour plots, darker contours correspond to larger values, and the zero contour is dashed.) The boundary conditions at the equator ($y = 0$) are complete cross-equatorial symmetry of the geometry, forcing and dynamics. To maximize the grid resolution in the regions of sloping bottom topography (which are of primary interest) the widths of the continental shelves have been greatly exaggerated; altogether they cover more than half the total area.

The flow is driven by a prescribed eastward wind stress $\tau(y)$. This stress corresponds to an infinite torque in water of vanishing depth unless frictional bottom torque is taken into account. (Recall that we view the ϵ-friction as a true Rayleigh friction, and not a bottom drag.) We recognize the importance of bottom friction in shallow water by assuming that, in nondimensional depths less than (say) b, an increasing proportion of the surface stress is transmitted directly to the bottom by waves and other phenomena not contained in the model, and does not act to accelerate the flow. These ideas are expressed by the assumption

$$y\bar{v}_E = -\frac{\tau(y)}{(H + b)} \tag{6.2}$$

where b is the nondimensional depth at which bottom stress becomes important. In all the solutions discussed b = .1 (about 400 meters), and the zonal wind stress takes the double-gyre form

$$\tau = \frac{2}{\pi} \sin^2\left(\frac{1}{2}\pi y\right) \tag{6.3}$$

or the triple-gyre form

$$\tau = -\tfrac{1}{2} \sin(\pi y) \sin(\tfrac{1}{2}\pi y). \tag{6.4}$$

Refer to Figure 1c. In both cases, both $\tau(y)$ and its derivative vanish at the latitudinal boundaries $y = 0, 2$. The double-gyre wind (6.3) was selected for its simplicity. The triple-gyre wind (6.4) agrees better with observations (e.g. Hellerman and Rosenstein, 1983).

The nondimensional surface heat flux Q is related to the dimensional surface heat flux Q_d by

$$Q = \frac{gk}{\rho_0 C_P f_0 U^2} Q_d \qquad (6.5)$$

where k is the coefficient of thermal expansion and C_P the heat capacity of seawater. Observations show that Q_d is of order ± 25 watt m^{-2} in mid-basin (but very noisy, and taking much larger values in localized regions) corresponding to a Q of order ± 30. However, in many solutions I have taken $Q \equiv 0$ (i.e. purely mechanical forcing.)

Since the S-equation (4.31) originates from (4.16), the volume-integrated temperature remains constant if Q integrates to zero. However, time-stepping experiments show that small numerical errors cause a steady, monotonic drift in the average temperature. To compensate for this drift, I have added a uniform heating per unit volume to the right-hand side of (4.31, 6.6) that is proportional to the difference between the total heat content of the ocean and a prescribed value. (More precisely, I prescribe the area-average of the upper-layer depth, $\langle h \rangle$.) At equilibrium, this uniform heating is very small, but it prevents the slow monotonic drift of temperature. The need for such a device is especially clear in the limit of two homogeneous layers, in which many workers since Parsons (1969) have recognized the need to prescribe the total volume of the warm layer as an independent parameter of the problem. We shall see that $\langle h \rangle$ exerts a profound control on the equilibrium circulation through its influence on the Rossby phase speed c.

In all the solutions presented, the resolution is 100×200 gridpoints, and the friction and diffusion coefficients have the values $\epsilon = .015$ and (with the single exception noted below) $\kappa = .1$, the smallest values for which smooth solutions could be obtained in all cases. I solved the GTLE (4.4, 31) by two distinct methods. In the first method, I stepped S forward in time using (4.31), and, at each time, calculated ψ from (4.4) by a method of simultaneous relaxation around closed concentric circuits beginning with the circuit of gridpoints just inside the boundary. This time-stepping method always converged to steady flow, but only after tens of thousands of time-steps. In the second method, both (4.4) and the steady form of (4.31) were simultaneously relaxed (the latter using an ADI method). To ensure a stable convergence, I rewrote (4.31) in the form

$$\mathbf{v}_1 \cdot \nabla S + \mathbf{v}_2 \cdot \nabla(S - H/Y) = \nabla \cdot [(\epsilon D + \kappa \mu)\nabla S + \mathbf{j}(\epsilon E + \kappa \alpha)] + Q + W_s \quad (6.6)$$

(where $\mathbf{v}_1$ and $\mathbf{v}_2$ collect many terms in (4.31)), and used Leonard's (1984) third-order upwind differencing scheme for the terms on the left-hand side of (6.6). Leonard's
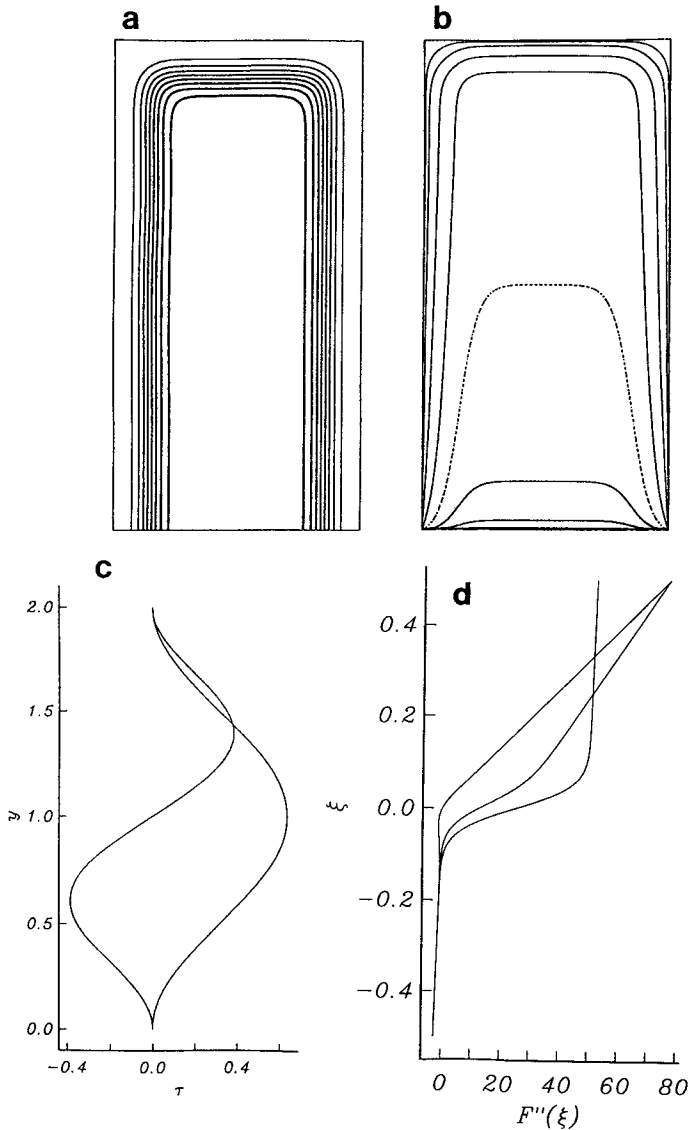
Figure 1. (a) The ocean depth $H(x, y)$, which ranges between zero at the coastlines and unity in mid-ocean. (b) The corresponding contours of H/y. (c) The zonal wind stress $\tau(y)$ for the two-gyre and three-gyre cases. (d) The temperature profile functions (6.8) and (6.14–15).

scheme damps grid oscillations without the excessive numerical diffusion of first-order upwind differencing. For small ϵ and κ, (under-) relaxation coefficients as low as .1 were sometimes required, but the solutions still converged much faster than by time-stepping, in the order of thousands of relaxation steps. The best strategy is to

begin with relatively large values of ϵ and κ, relax the GTLE to equilibrium, reduce ϵ and κ, and then relax to the final equilibrium. In all the solutions described, I first solved the GTLE on a coarse grid of 50×100 points, and then transferred to the finer grid of 100×200 points for further relaxation at lower values of the friction and diffusion.

We begin by briefly considering the solutions for homogeneous flow $\theta \equiv 0$, for which the GTLE reduce to a single linear equation for the transport streamfunction,

$$J\left(\frac{y}{H}, \psi\right) = -W(x, y) + \nabla \cdot \left(\frac{\epsilon}{H} \nabla \psi\right). \tag{6.7}$$

As noted by Salmon (1992, Sec. 3), it is best to regard (6.7) as an advection/diffusion equation for the scalar ψ in which y/H is the "streamfunction" of the advecting "velocity," and $-W$ is the "source." Thus, for the bathymetry of Figure 1a, ψ is advected westward along "streamlines" (Fig. 1b) that emanate from a single point on the eastern boundary at the equator, and converge to the equatorial point on the western boundary. If W is negligible near the boundaries, then, as $\epsilon \to 0$, there are no boundary layers or internal boundary layers in the solutions of (6.7), and the ϵ-diffusion in (6.7) is important only near the western equatorial point of convergence.

Figure 2b and 2c show the solution of (6.7) for the wind curl corresponding to the double-gyre case (6.3) and the triple-gyre case (6.4), respectively. In Figures 2b–c we see how the ψ-values built up by wind torque in the flat-bottomed interior ocean are carried westward along y/H-lines toward the equatorial convergence point, yielding the pattern of western continental-slope currents and counter-currents discussed by Salmon (1992). These currents are controlled solely by y/H, and are asymptotically independent of ϵ. The corresponding flat-bottomed ($H \equiv 1$) solution, with its ϵ-thickness western boundary layers (here corresponding to 1.5 grid-separation distances) is shown in Figure 2a. As emphasized by Kawase (1993), these equatorial-basin solutions differ significantly from the corresponding solutions in a non-equatorial basin with a southern coastal boundary, as $\epsilon \to 0$. In the latter case, ψ is swept around the closed contours of y/H, and its (nearly constant) value on each contour is determined by the very small diffusion across contours throughout the basin (see Batchelor (1956) and Rhines and Young (1983) for a discussion of this type of problem). However, southern coastal boundaries are unrealistic, and we consider only the equatorial case.

We now consider a series of cases with non-uniform θ, corresponding to various values of the temperature profile function F'' and prescribed average upper-layer thickness $\langle h \rangle$. Table 1 summarizes the solutions. Figure 1d shows the profile functions. We begin with a solution (solution A) corresponding to the double-gyre
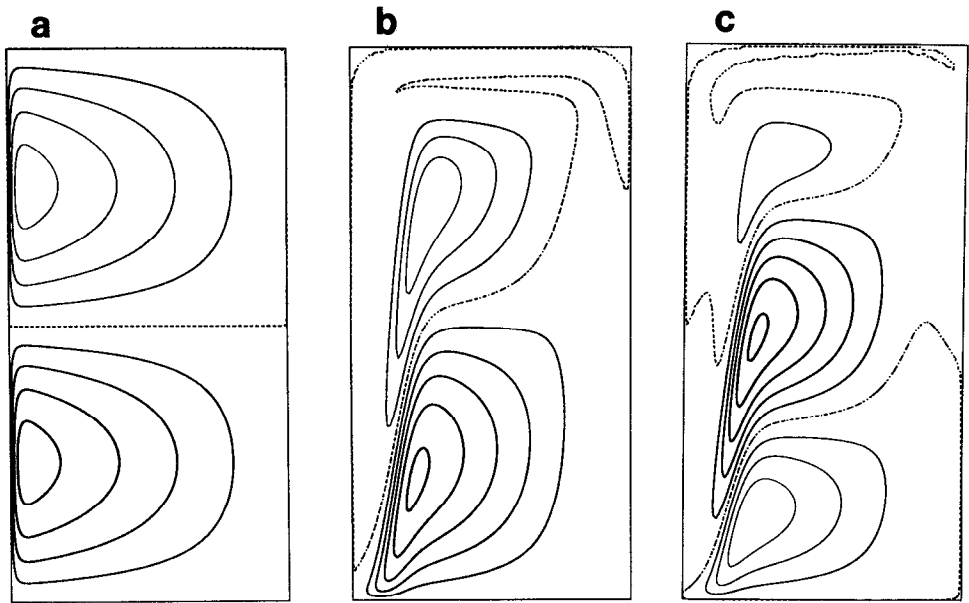
Figure 2. Homogeneous-flow solutions, $\theta \equiv 0$. The transport streamfunction ψ satisfying (6.7) with wind curl W corresponding to the two-gyre wind (a) in an ocean of uniform depth, $H \equiv 1$ (range: $\psi = -.783$ to $+.783$); and (b) for the bathymetry in Figure 1a (range: $-.386$ to $+.530$). (c) The streamfunction corresponding to the bathymetry in Figure 1a and the three-gyre wind (range: $-.486$ to $+.662$). Darker contours correspond to larger values, and the zero contour is dashed.

wind (6.3), no solar heating ($Q \equiv 0$), $\langle h \rangle = .1$, and the profile function

$$F''(\xi) = 5\xi + 50\Lambda(\xi) \tag{6.8}$$

corresponding to two (nearly) homogeneous layers with a relatively small uniform background stratification. The temperature jump between layers is 50, and $\Lambda(\xi)$ is the smooth approximation to the Heaviside function defined by (2.35). Here, and in

Table 1. Summary of solutions.

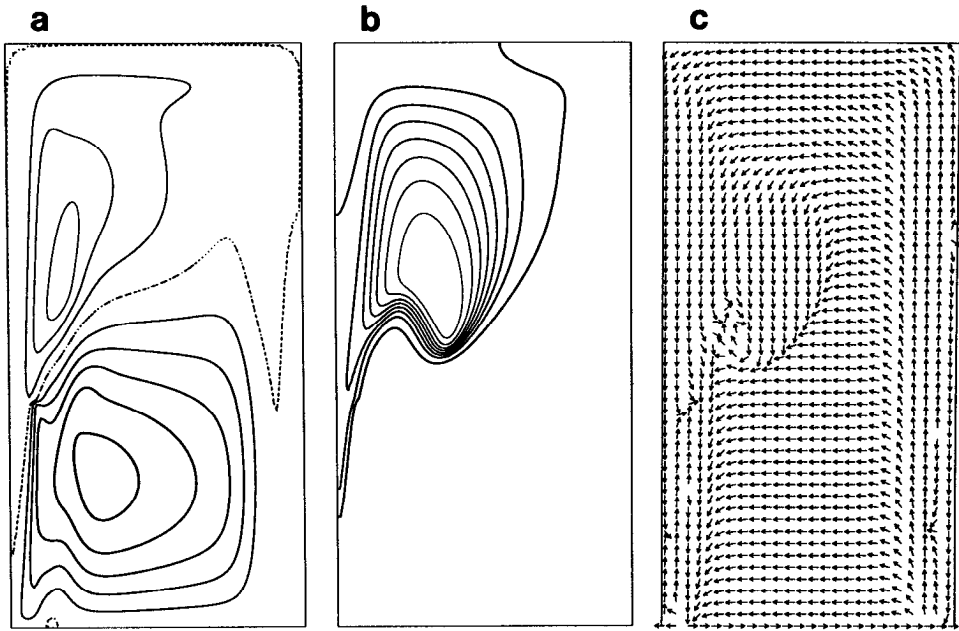| Solution	gyres	F''	$\langle h \rangle$	Ekman heat transport?	Solar heating?	κ
A	2	$5\xi + 50\Lambda(\xi)$	.1	yes	no	.1
B	2	$5\xi + 50\Lambda(\xi)$	.1	no	no	.1
C	2	$5\xi + 50\Lambda(\xi)$	.05	no	no	.1
D	2	$5\xi + 50\Lambda(\xi)$	.15	no	no	.1
E	2	$5\xi + 150\xi\Lambda(\xi)$	.15	no	no	.1
F	3	$5\xi + (25 + 100\xi)\Lambda(\xi)$	.1	no	no	.1
G	3	$5\xi + (25 + 100\xi)\Lambda(\xi)$	.1	no	yes	.15

a   **b**   **c**

Figure 3. The (a) transport streamfunction (range: $-.574$ to $+.883$); (b) surface temperature (9.29 to 51.8); and (c) characteristic velocity v_c in solution A. The arrows in (c) have been normalized to have the same length.

all the solutions presented, I have taken $d = .05$ in (2.35) and $\delta = .5$ in (4.14). Thus the equatorial adjustment (4.13) to (1.1) is significant only in the southernmost quarter-basin.

Figure 3a shows the transport streamfunction ψ in solution A. The difference between Figures 2b and 3a is caused solely by the JEBAR-term in (4.4), but is quite significant; the total transport in Figure 3a is about 50% greater than that in Figure 2b. Now, rewrite (4.4) as

$$J\left(\psi, \frac{y}{H}\right) = \frac{1}{H^2} J(H, \gamma) + W - \nabla \cdot \left(\frac{\epsilon}{H} \nabla \psi\right) \qquad (6.9)$$

and define the *JEBAR torque*

$$J \equiv \frac{1}{H^2} J(H, \gamma). \qquad (6.10)$$

Wherever $H_y = 0$ (i.e. except near the northern boundary), this is

$$J = \frac{1}{H^2} H_x \gamma_y = -\frac{1}{H^2} H_x \int_{-H}^{0} z\theta_y \, dz \qquad (6.11)$$

which as $H \rightarrow 0$ becomes

$$J \approx \frac{1}{2} H_x \theta_y. \tag{6.12}$$

The limit (6.12) is useful for estimation. From either (6.11) or (6.12) we see that on the western continental slope, where $H_x > 0$, J has the same sign as θ_y. Calculations (not presented) show that the biggest J-values are negative and occur where the Gulf Stream leaves the continental slope. There, the large positive value of H_x combines with very large *negative* values of θ_y to yield a negative torque whose extremum coincides with the sharp curve in ψ near the western boundary, between gyres (Fig. 3a.)

Figure 3c shows the *characteristic velocity* in the S-equation (6.6), defined by

$$\begin{aligned}
\mathbf{v}_c &\equiv \mathbf{v}_1 + \mathbf{v}_2 \\
&= (W_T + W_B)[(-\psi_y, \psi_x) + (\tilde{c}, 0)] + W_B \tilde{c}_H (H_y, -H_x) + (c_e, 0) + Ekman
\end{aligned} \tag{6.13}$$

where *Ekman* stands for the terms representing the effect of the Ekman transport on the vertically-averaged temperature (the $\mathbf{v}_T$ and $\mathbf{v}_B$ terms in (4.31)), and all the other terms have been defined in Section 4. In Figure 3c, each vector has been normalized to the same length, to give the clearest possible indication of the direction in which S-information flows. The first three terms in (6.13) correspond to the advection of S by the depth-averaged flow, the westward propagation of S at the internal Rossby wave speed, and the propagation of S along isobaths, in the direction of topographic Rossby waves. The c_e-term is insignificant, except at the equator. The Ekman transport term is significant, and is responsible for the large southward component of $\mathbf{v}_c$ at northern mid-basin in Figure 3c. Figure 3c also shows a shock at the boundary between gyres, where these Ekman-dominated southward characteristic velocities in the subpolar gyre converge with the Rossby-dominated westward characteristic velocities in the subtropical gyre. The shock coincides with the outcrop of the main thermocline (Fig. 3b) and the paths of the separated western boundary current (Fig. 4a) and deep countercurrent (Fig. 4b).[6] The large upper-layer thickness south of the shock (see Fig. 8A) causes the Rossby speed c to be large there, leading to the westward characteristic velocities that contribute to the shock.

A second shock, trending north-northeast and perhaps following a line of constant H/y, is apparently present on the southwestern continental slope (Fig. 3c), where southward characteristic velocities bringing cold water from far north converge with the northward characteristic velocities in the Gulf Stream. This western-continental-slope shock ends abruptly at a point coincident with the tiny inflection in the warmest contour of Figure 3b, and is more apparent in the corresponding map of S (Fig. 10a).

---

6. In Figure 4 (and in all other maps of the horizontal velocity), the length of the arrows is proportional to the *square root* of the fluid speed, to keep the high-velocity arrows from dominating the picture. Arrows are drawn for only *one sixteenth* of the model gridpoints.
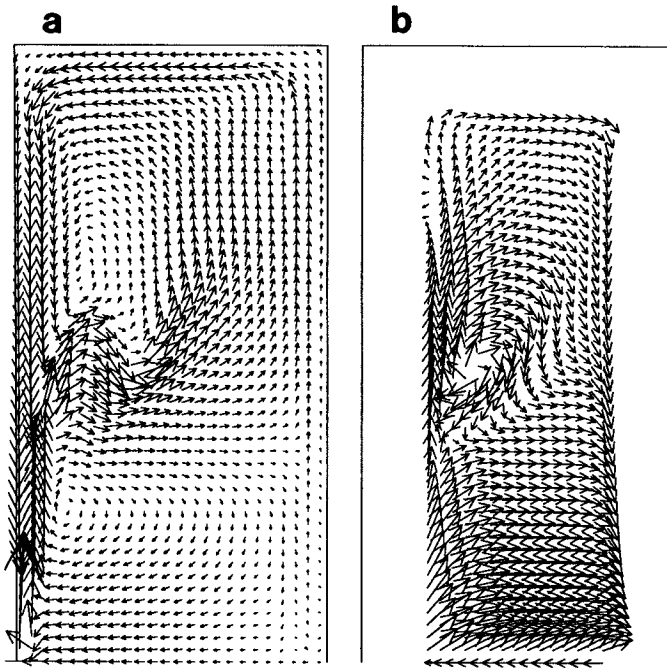
Figure 4. The horizontal velocity in solution A, (a) at the ocean surface (maximum velocity 679., rms = 42.8); and (b) at the ocean bottom (maximum = 11.6, rms = 3.74), in water deeper than .75. The length of each vector is proportional to the *square root* of the fluid speed. Velocities are in units of .2 km/day.

It appears in all of the solutions presented below. In contrast, the existence of the mid-ocean shock depends sensitively on the prescribed thermal structure (principally, on the prescribed volume of warm water). As we shall see, in none of the solutions in which both shocks are present do these two shocks connect; there is always a region between the shocks in which the characteristic velocity varies smoothly, and temperature flows freely between the gyres. This gap between the shocks coincides with the region in which the Gulf Stream flows down the continental slope.

The Ekman terms in (4.31) probably over-estimate the importance of Ekman heat transport. For example, if the Ekman layer transports cold surface water southward over warmer water at depth (as in solution A), then the resulting vertical mixing would reduce the net horizontal heat transport well below that estimated by (4.28). Figure 5 shows the surface temperature, characteristic velocity v_c, and surface velocity in solution B, which differs from A only in that the Ekman heat-transport terms have been dropped from (4.31) and (6.13). From Figure 5b, we see that the mid-ocean shock has disappeared, and the characteristic velocity is westward over nearly the whole interior ocean. There is no rapid mid-ocean change in the surface
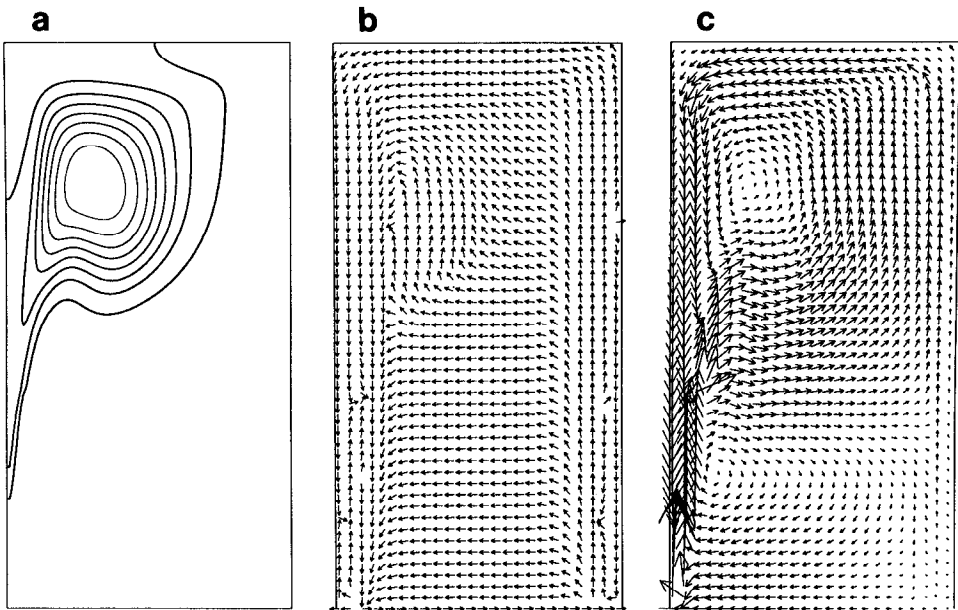
a   **b**   **c**

Figure 5. The (a) surface temperature (range: 7.24 to 51.7); (b) normalized characteristic velocity v_c; and (c) surface velocity (maximum = 673., rms = 41.5) in solution B, which differs from A only in the neglect of Ekman heat transport.

temperature (Fig. 5a), and the westward drift is correspondingly diffuse (Fig. 5c). All the remaining solutions omit the Ekman heat transport.

We next consider solutions with the same two-gyre wind stress (6.3) and two-homogeneous-layers profile function (6.8), but with different prescribed values of the average upper-layer thickness $\langle h \rangle$. Solution C differs from B only in its lower prescribed upper-layer thickness, $\langle h \rangle = .05$, but the differences in the temperature and velocity fields are dramatic. The smaller volume of warm water reduces the Rossby speed c, especially in the subpolar gyre, where the characteristic velocity is eastward and dominated by ψ (Fig. 6b). The main thermocline outcrops sharply at a mid-ocean shock (Fig. 6a). South of the outcrop, the relatively large upper-layer thickness causes the characteristic velocities to be westward. The surface velocity (not shown) is similar to that in solution A, and the bottom velocity (Fig. 6c) has a strong component parallel to the shock. Solution C, with its isolated, southward western boundary current in the subpolar gyre, closely resembles the theoretical model of Veronis (1973). Temperature sections (Fig. 9) reveal the warm water flowing northward along the eastern boundary, westward along the northern boundary (Fig. 8C), and southward along the western boundary.

Solution D differs from B and C only in its much larger $\langle h \rangle = .15$. Now, however, the Rossby speed c completely dominates the characteristic velocity, which is westward throughout the mid-ocean (Fig. 7b). The area of cold-water outcrop is
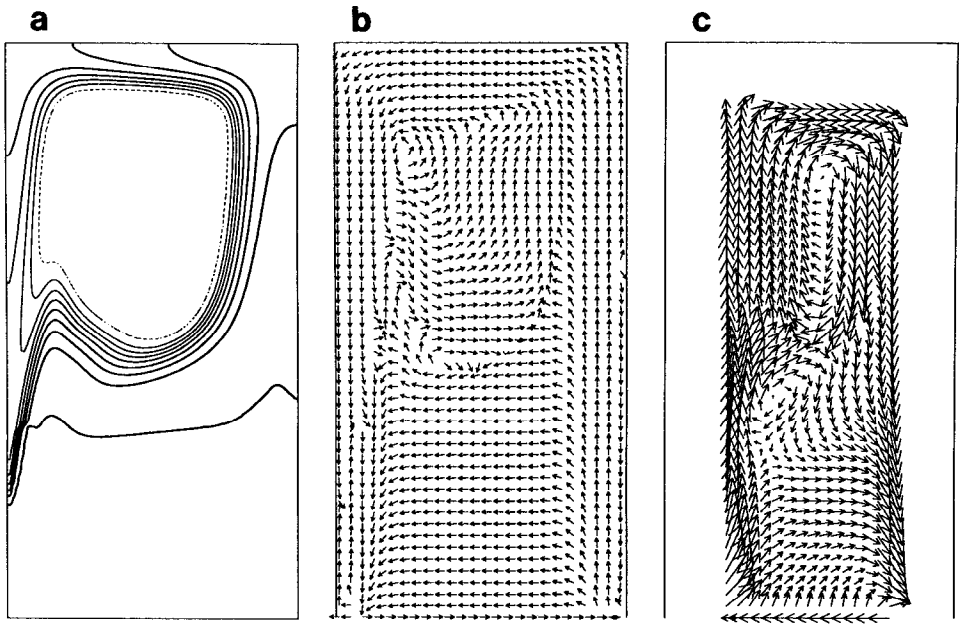
Figure 6. The (a) surface temperature (range: -5.52 to 51.3); (b) normalized v_c; and (c) horizontal velocity at the ocean bottom (maximum $= 10.0$, rms $= 2.53$) in solution C, which differs from A and B in its lower prescribed average upper-layer depth $\langle h \rangle = .05$.

swept westward (Fig. 7a) and greatly diminished, and the abyssal flow is eastward nearly everywhere (Fig. 7c).

Do these numerical solutions resemble the analytical solution for two-layer flow along a western continental slope offered by S92? Figure 10 shows the upper-layer potential vorticity $q_1 \equiv S$ and lower-layer potential vorticity $q_2 \equiv S - H/Y$ in solution A. (Note that the definition of potential vorticity is here modified slightly, by replacing y with Y.) As predicted in S92, a line of constant H/y separates a shoreward region of uniform q_2, in which q_1 changes rapidly, from a region of relatively uniform q_1, in which q_2 changes rapidly. However, the Rayleigh friction ϵ is too large to make a really meaningful comparison; for $\epsilon = .015$, the predicted $\epsilon^{1/2}$-thickness internal boundary layer separating the two regions has a thickness $(.12)$ comparable to the width of the continental slope. Thus the numerical calculations are far from the asymptotic limit $\epsilon \to 0$ considered in the previous paper. In fact, the solutions shown here with 100×200 resolution differ significantly from corresponding solutions on the 50×100 grid (and with slightly larger values of ϵ and κ), offering further evidence that the numerical solutions are far outside the asymptotic regime. Unfortunately, the numerical solutions diverged for ϵ less than a grid distance, indicating that unresolved ϵ-thickness boundary layers are a problem even when they are not required by the particular forcing and basin geometry under consideration. As noted
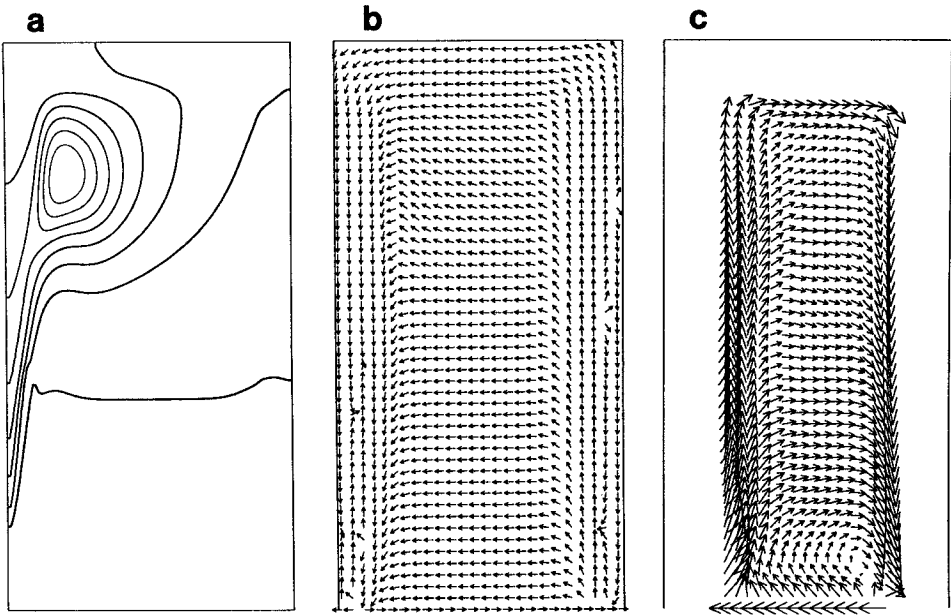
Journal of Marine Research

a   **b**   **c**

Figure 7. The same as Figure 6, but for solution D, in which $\langle h \rangle$ = .15. (a) Surface temperature (42.5 to 52.2); (b) normalized v_c; (c) bottom velocity (maximum = 6.2, rms = 1.7).

by Jarvis and Veronis (1994), the mid-ocean shocks also have a thickness $\epsilon^{1/2}$. This is in contrast to Parson's (1969) calculation, in which the lower layer is quiescent, the upper layer carries the full Sverdrup transport, and the separated western boundary layer has thickness ϵ.

Next we examine a solution (solution E) with the profile function

$$F''(\xi) = 5\xi + 150\xi\Lambda(\xi) \qquad (6.14)$$

corresponding to a jump in θ_z, but not θ, at the thermocline $\xi = 0$. See Figure 8E. Figure 11 shows the transport streamfunction and surface temperature. Because there is no vertical jump in temperature, the characteristic velocity (not shown) varies smoothly, and no mid-ocean shocks occur.

Our last two solutions (F and G) use the more realistic three-gyre wind (6.4), and the profile function

$$F''(\xi) = 5\xi + (25 + 100\xi)\Lambda(\xi) \qquad (6.15)$$

corresponding to a jump in both temperature θ and stratification θ_z at the thermocline. In both solutions, the prescribed upper-layer thickness is $\langle h \rangle$ = .1. In solution F, as in all previous solutions, the surface heat flux vanishes ($Q \equiv 0$). In solution G,
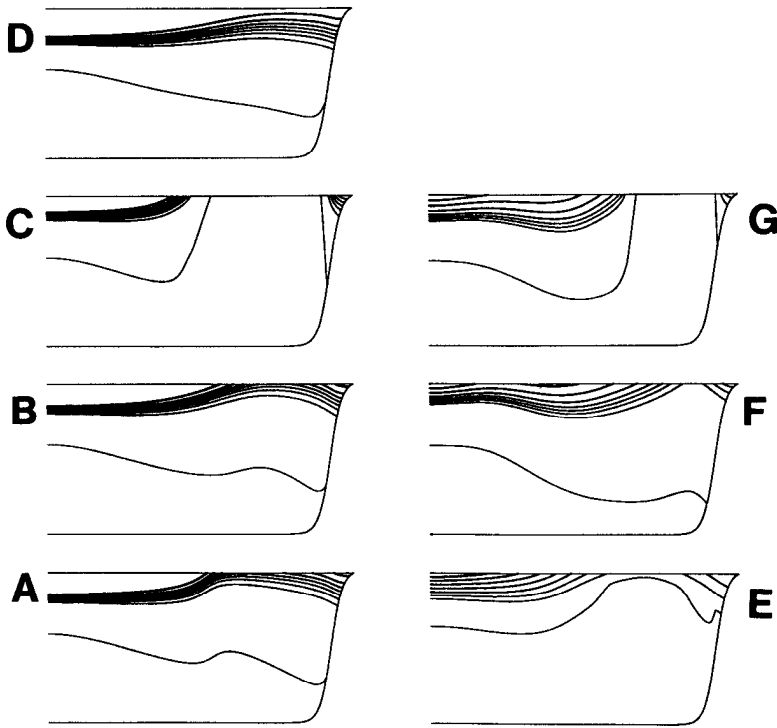
Figure 8. The temperature in a north-south section from the equator (left) to the northern boundary in each of the numerical solutions, A through G. The base of the main thermocline corresponds to zero temperature, and the temperature ranges are: (A) $\theta = -8.29$ to $+51.7$; (B) -8.29 to $+51.7$; (C) -8.71 to $+51.3$; (D) -7.88 to $+52.1$; (E) -7.99 to $+62.0$; (F) -8.80 to $+50.1$; (G) -9.39 to $+57.9$.

however,

$$Q = 30 \frac{H}{H + b} \cos\left(\frac{\pi}{2} y\right)$$
(6.16)

corresponding to net heating in the southern half-basin and net cooling in the north. Analysis of (4.31) shows that Q *must* vanish as $H \to 0$; that is, horizontal heat fluxes

Figure 9. The temperature in east-west sections in solution C at (a) $y = .5$ (temperature range: -6.1 to 51.1); (b) $y = .75$ (-5.1 to 50.6); and (c) $y = 1.5$ (-8.5 to 46.6).
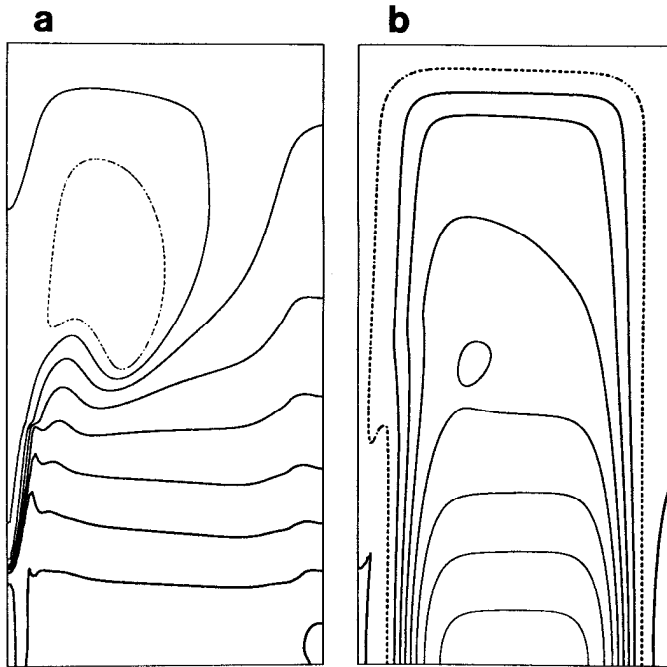
Figure 10. The (a) upper-layer potential vorticity S; and (b) lower-layer potential vorticity $S - H/Y$ in solution A.

cannot balance a net surface flux in water of vanishing depth. The quotient in (6.16) expresses the idea that the various contributors to the net surface flux achieve a local balance as the ocean depth decreases past $b = .1$. This assumption is obviously quite arbitrary.

With the nonvanishing surface flux (6.16) and $\kappa = .1$ (as in solutions A through F), the numerical solutions diverged. However, the solution converged for $\kappa = .15$. Thus solution G differs from F only in its heat flux (6.16), and its larger value of temperature diffusivity. However, the differences in the flow are quite dramatic. In solution F, predominantly westward characteristic velocities (not shown) press the warm water against the western coast (Fig. 12). In solution G, the strongly eastward characteristic velocities in the colder subpolar gyre create a shock (Fig. 13) resembling that in solution C. The surface velocity (Fig. 14a) separates sharply from the western slope, but the eastward drift is relatively diffuse. The deep flow is westward on both flanks of the North Atlantic Current (Fig. 14b).

7. Remarks

The planetary geostrophic equations (PGE), (4.1–2) with boundary conditions of no-normal-flow and prescribed heat flux, are the simplest conceivable "balanced" dynamics—simpler even than the quasigeostrophic equations in that the PGE
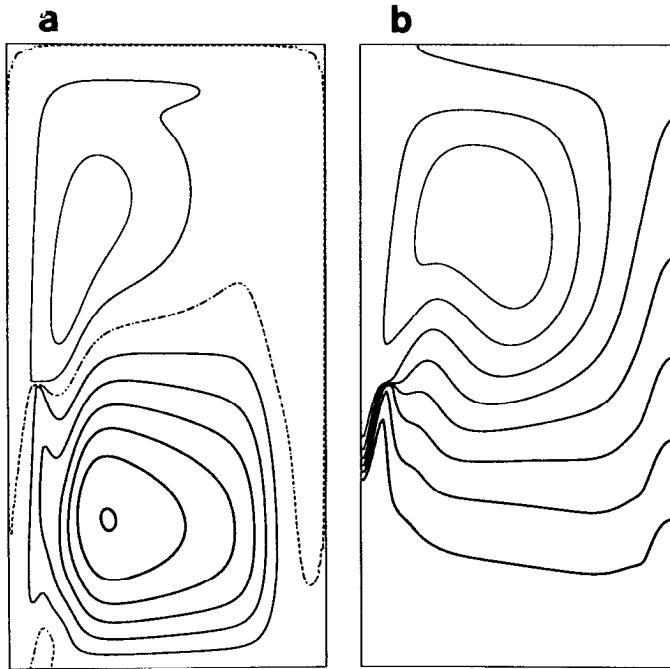
Figure 11. The (a) transport streamfunction (range $-.457$ to $.930$); and (b) surface temperature ($.05$ to 62.6) in solution E.

entirely omit all three components of the inertia. However, the PGE are superior to the quasigeostrophic equations in that they are not restricted to flows which remain near a prescribed rest state with nearly flat isopycnals, or to ocean basins with a nearly flat bottom. In contrast to the quasigeostrophic equations and other, more sophisticated balanced approximations, the PGE cannot satisfy no-normal-flow boundary conditions in the absence of friction. But the friction is really only required at *vertical* sidewalls, or along the coastal boundary of vanishing depth in an ocean with non-vertical boundaries. (Of course, as in all models, dissipation is also required to prevent advection from building up infinitely large gradients of temperature as time increases.)

Numerical experiments suggest that (at least in parameter ranges of practical interest) the PGE approach a steady state. This fact greatly simplifies the analysis of solutions, and it justifies the first of two assumptions used here to reduce the number of independent variables from four to two. The other assumption, (1.1), is much more questionable, but it is more general and convenient than the common assumption of two homogeneous layers, and many workers have noted a tendency for the potential vorticity to be uniform on isopycnal surfaces. Indeed, the iso-lines on meridional hydrographic sections often resemble rays emanating from a "point" on the equator, as required by (1.1).
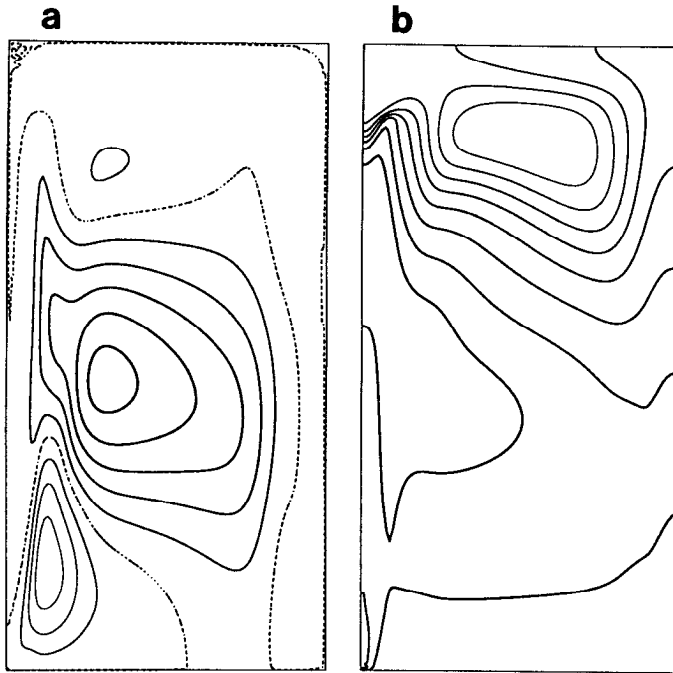
Figure 12. The (a) transport streamfunction (range −.735 to +1.10); and (b) surface temperature (2.42 to 50.6) in solution F.

Of course, a theory *based* upon the assumption of uniform potential vorticity can hardly explain why the potential vorticity tends to be uniform. Neither can the generalized two-layer equations (GTLE), in which the vertical profile of temperature is severely constrained by the choice of profile function $\Theta(\ )$, explain the *existence* of the main thermocline, the midwater layer in which the temperature and its derivative change rapidly. Stommel and Webster (1962), Young and Ierley (1986), and Salmon (1990) have suggested that the main thermocline is an internal boundary layer in solutions of the full, three-dimensional PGE, and Salmon and Hollerbach (1991, Sec. 8) give analytical solutions, containing internal boundary layers, in which the flow resembles that in subtropical gyres. But although these studies offer theoretical justification for a profile function with a relatively sharp jump, one can seriously question whether it really makes sense to *prescribe* such an important feature of the physics.

Solutions of the full, three-dimensional PGE also reveal the formation of large regions of static instability, unless an explicit vertical convective mixing is imposed. This seems to be a property of all balanced dynamical approximations in which the vertical derivative of density is free to change sign (including even the primitive equations, in which the *only* balance is hydrostatic), but the problem seems especially acute for the PGE. Numerical experiments (Zhang *et al.,* 1992) show that, without a
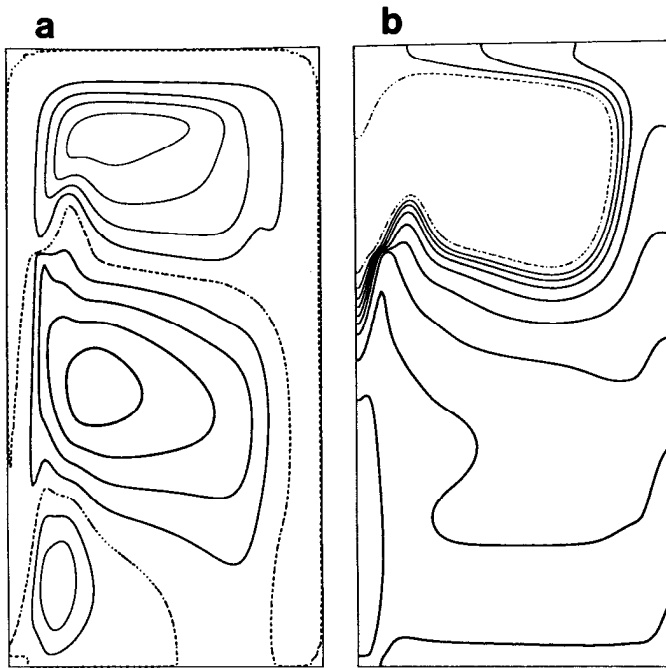
Figure 13. The (a) transport streamfunction (range $-.992$ to $+1.06$); and (b) surface temperature (-6.55 to $+58.1$) in solution G.

convective adjustment, the warmest water can fill up the deep ocean. The GTLE avoid the need for a convective adjustment by using a statically stable profile function, thereby "projecting out" the physics leading to static instability, but, again, one can question the physical justification for this approach (although it is not obviously more arbitrary than the convective adjustment imposed on primitive equation models).

The primary reason for studying the PGE, and the GTLE in particular, is that their mathematical simplicity offers great hope for physical understanding. The general analytical solutions in Section 3 are a particularly encouraging hint of what might eventually be possible. Moreover, I suspect that the complicated topography of the ocean basins may be exerting a strong but very non-local control on the time-average flow, and that it is more important to model this topographical control accurately than it is to take account of the inertia.

Although the numerical solutions described in Section 6 offer some encouragement, real physical understanding likely demands consideration of the asymptotic limit of small dissipation, and as already conceded, the numerical solutions lie far outside this asymptotic regime. The fundamental difficulty seems to be the disparity in the boundary layer thicknesses, ϵ and $\epsilon^{1/2}$, as $\epsilon \rightarrow 0$. Jarvis and Veronis (1994) recognized this difficulty and overcame it with a much finer grid resolution near the
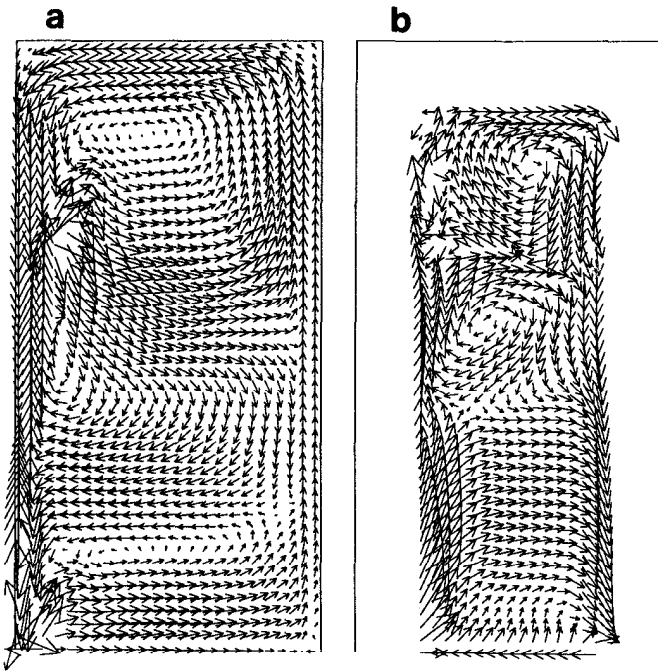
Figure 14. The horizontal velocity (a) at the surface (maximum = 198., rms = 26.6); and (b) at the ocean bottom in water deeper than .75 (maximum = 7.3, rms = 2.0) in solution G.

boundaries, but their method may not apply easily to the case of realistic coastline geometry. However, in their ideal form (2.17, 19), the GTLE are "non-metric"; that is, they contain only Jacobian derivatives. This may make it possible to solve the GTLE on a non-orthogonal grid using the natural variables H and y as new independent variables, particularly if the dissipation terms in (4.4, 4.31) could be replaced by dissipation terms taking a simpler form in the new coordinates, or—better yet—if the equations could then be solved entirely without dissipation and the resulting multivalued-ness resolved by jump conditions in the usual manner of obtaining weak solutions. The use of ocean depth H as an independent variable would make it much easier to accommodate real bathymetry, and would naturally concentrate numerical resolution in regions of steeply sloping topography, where observations typically reveal strong, narrow currents. I speculate that the use of realistic bathymetry and smaller (or no) dissipation will dramatically improve the resemblance between numerical solutions of the GTLE and oceanographic observations. Ultimately, it will certainly be necessary to consider PGE models with more than two vertical degrees of freedom, but the simplicity of the GTLE should first be fully exploited. This simplicity, and the hope it offers for a completely deductive theory, are the primary advantages of the GTLE.

REFERENCES

Batchelor, G. K. 1956. Steady laminar flow with closed streamlines at large Reynolds number. J. Fluid Mech. *1,* 177–190.

Cushman-Roisin, B. 1984. On the maintenance of the subtropical front and its associated countercurrent. J. Phys. Oceanogr., *14,* 1179–1190.

de Szoeke, R. A. 1985. Wind-driven mid-ocean baroclinic gyres over topography: A circulation equation extending the Sverdrup relation. J. Mar. Res., *43,* 793–824.

Dewar, W. K. 1987. Planetary shock waves. J. Phys. Oceanogr., *17,* 470–482.

—— 1991. Arrested fronts. J. Mar. Res., *49,* 21–52.

—— 1992. Spontaneous shocks. J. Phys. Oceanogr., *22,* 505–522.

Ford, R. 1992. Generalized two-layer planetary geostrophic equations, *in* Dynamics of the Outer Planets, G. Flierl, ed. (1992 GFD proceedings, WHOI technical report WHOI-93-24.) 205–228.

Hellerman, S. and M. Rosenstein. 1983. Normal monthly wind stress over the world ocean with error estimates. J. Phys. Oceanogr., *13,* 1093–1104.

Hoskins, B. J., M. E. McIntyre and A. W. Robertson, 1985. On the use and significance of isentropic potential vorticity maps. Q. J. Roy. Met. Soc., *111,* 877–946.

Ierley, G. R. and W. R. Young. 1983. Can the western boundary layer affect the potential vorticity distribution in the Sverdrup interior of a wind-gyre? J. Phys. Oceanogr., *13,* 1753–1763.

Jarvis, R. A. and G. Veronis. 1994. Strong deep recirculations in a two-layer wind-driven ocean. J. Phys. Oceanogr. *24,* 759–776.

Kamenkovich, V. M. and G. M. Reznik. 1972. A contribution to the theory of stationary wind-driven currents in a two-layer liquid. Izv. Atmos. Ocean. Phys. *8,* 419–34. (English transl. Atmos. Ocean Phys., *8,* 238–245.)

Kawase, M. 1993. Effects of a concave bottom geometry on the upwelling-driven circulation in an abyssal ocean basin. J. Phys. Oceanogr., *23,* 400–405.

Leonard, B. P. 1984. Third-order upwinding as a rational basis for computational fluid dynamics, *in* Computational Techniques and Applications: CTAC-83, J. Noye & C. Fletcher, eds., Elsevier North-Holland, 106–120.

Luyten, J., J. Pedlosky and H. Stommel. 1983. The ventilated thermocline. J. Phys. Oceanogr., *13,* 293–309.

Luyten, J. and H. Stommel. 1986. Gyres driven by combined wind and buoyancy flux. J. Phys. Oceanogr., *16,* 1551–1560.

Needler, G. T. 1971. Thermocline models with arbitrary barotropic flow. Deep-Sea Res., *18,* 895–903.

Parsons, A. T. 1969. Two layer model of Gulf Stream separation. J. Fluid Mech., *39,* 511–528.

Rhines, P. B. and W. R. Young. 1982. A theory of wind-driven circulation. I. Mid-ocean gyres. J. Mar. Res., *40* (Suppl.), 559–596.

—— 1983. How rapidly is a passive scalar mixed within closed streamlines? J. Fluid Mech., *133,* 133–145.

Salmon, R. 1986. A simplified linear ocean circulation theory. J. Mar. Res., *44,* 695–711.

—— 1990. The thermocline as an "internal boundary layer." J. Mar. Res., *48,* 437–469.

—— 1992. A two-layer Gulf Stream over a continental slope. J. Mar. Res., *50,* 341–365.

Salmon, R. and R. Hollerbach. 1991. Similarity solutions of the thermocline equations. J. Mar. Res., *49*, 249–280.

Stommel, H. 1948. The western intensification of wind-driven currents. Am. Geophys. Union Trans., *29*, 202–206.

Stommel, H. and J. Webster. 1962. Some properties of thermocline equations in a subtropical gyre. J. Mar. Res., *20*, 42–56.

Veronis, G. 1973. Model of world ocean circulation. I. Wind-driven, two-layer. J. Mar. Res., *31*, 228–288.

Welander, P. 1971. Some exact solutions to the equations describing an ideal-fluid thermocline. J. Mar. Res., *29*, 60–68.

Whitham, G. B. 1974. Linear and Nonlinear Waves. John Wiley, New York 636 pp.

Young, W. R. and G. R. Ierley. 1986. Eastern boundary conditions and weak solutions of the ideal thermocline equations. J. Phys. Oceanogr., *16*, 1884–1900.

Young, W. R. and P. B. Rhines. 1982. A theory of the wind-driven circulation II. Gyres with western boundary layers. J. Mar. Res., *40*, 849–872.

Zhang, S., C. A. Lin and R. J. Greatbatch. 1992. A thermocline model for ocean-climate studies. J. Mar. Res., *50*, 99–124.